The Astrophysical Journal, 599:847–864, 2003 December 20
© 2003. The American Astronomical Society. All rights reserved. Printed in U.S.A.

THE REST-FRAME OPTICAL LUMINOSITY DENSITY, COLOR, AND STELLAR MASS DENSITY OF THE UNIVERSE FROM $z = 0$ TO $z = 3$[1]

Gregory Rudnick,[2] Hans-Walter Rix,[3] Marijn Franx,[4] Ivo Labbé,[4] Michael Blanton,[5] Emanuele Daddi,[6] Natascha M. Förster Schreiber,[4] Alan Moorwood,[6] Huub Röttgering,[4] Ignacio Trujillo,[3] Arjen van de Wel,[4] Paul van der Werf,[4] Pieter G. van Dokkum,[7] and Lottie van Starkenburg[4]

Received 2003 July 5; accepted 2003 September 7

ABSTRACT

We present the evolution of the rest-frame optical luminosity density $j_\lambda^{\rm rest}$, the integrated rest-frame optical color, and the stellar mass density, ρ_*, for a sample of K_s band–selected galaxies in the Hubble Deep Field–South (HDF-S). We derived $j_\lambda^{\rm rest}$ in the rest-frame U, B, and V bands and found that $j_\lambda^{\rm rest}$ increases by a factor of 1.9 ± 0.4, 2.9 ± 0.6, and 4.9 ± 1.0 in the V, B, and U rest-frame bands, respectively, between redshifts of 0.1 and 3.2. We derived the luminosity-weighted mean cosmic $(U-B)_{\rm rest}$ and $(B-V)_{\rm rest}$ colors as a function of redshift. The colors bluen almost monotonically with increasing redshift; at $z = 0.1$, the $(U-B)_{\rm rest}$ and $(B-V)_{\rm rest}$ colors are 0.16 and 0.75, respectively, while at $z = 2.8$ they are -0.39 and 0.29, respectively. We derived the luminosity-weighted mean M/L_V^*, using the correlation between $(U-V)_{\rm rest}$ and $\log M/L_V^*$ that exists for a range in smooth star formation histories (SFHs) and moderate extinctions. We have shown that the mean of individual M/L_V^* estimates can overpredict the true value by ~70%, while our method overpredicts the true value by only ~35%. We find that the universe at $z \sim 3$ had ~10 times lower stellar mass density than it does today in galaxies with $L_V^{\rm rest} > 1.4 \times 10^{10}\ h_{70}^{-2}\ L_\odot$. Half of the stellar mass of the universe was formed by $z \sim 1$–1.5. The rate of increase in ρ_* with decreasing redshift is similar to but above that for independent estimates from the HDF-N, but it is slightly less than that predicted by the integral of the SFR(z) curve.

Subject headings: galaxies: evolution — galaxies: formation — galaxies: high-redshift — galaxies: stellar content

On-line material: color figures

1. INTRODUCTION

A primary goal of galaxy evolution studies is to elucidate how the stellar content of the present universe was assembled over time. Enormous progress has been made in this field over the past decade, driven by advances over three different redshift ranges. Large-scale redshift surveys with median redshifts of $z \sim 0.1$, such as the Sloan Digital Sky Survey (SDSS; York et al. 2000) and the 2dF Galaxy Redshift Survey (2dFGRS; Colless et al. 2001), coupled with the near-infrared (NIR) photometry from the Two Micron All-Sky Survey (2MASS; Skrutskie et al. 1997), have recently been able to assemble the complete samples, with significant comoving volumes, necessary to establish crucial local reference points for the local luminosity function (e.g., Folkes et al. 1999; Blanton et al. 2001, 2003b, the latter hereafter B03; Norberg et al. 2002) and the local stellar mass function of galaxies (Cole et al. 2001; Bell et al. 2003a).

At $z \lesssim 1$, the pioneering study of galaxy evolution was the Canada-France Redshift Survey (CFRS; Lilly et al. 1996). The strength of this survey lay not only in the large numbers of galaxies with confirmed spectroscopic redshifts but also in the I-band selection, which enabled galaxies at $z \lesssim 1$ to be selected in the rest-frame optical, the same way in which galaxies are selected in the local universe.

At high redshifts the field was revolutionized by the identification, and subsequent detailed follow-up, of a large population of star-forming galaxies at $z > 2$ (Steidel et al. 1996). These Lyman break galaxies (LBGs) are identified by the signature of the redshifted break in the far-UV continuum caused by intervening and intrinsic neutral hydrogen absorption. There are over 1000 spectroscopically confirmed LBGs at $z > 2$, together with the analogous U-dropout galaxies identified using *Hubble Space Telescope* (*HST*) filters. The individual properties of LBGs have been studied in great detail. Estimates for their star formation rates (SFRs), extinctions, ages, and stellar masses have been made by modeling the broadband fluxes (Sawicki & Yee 1998, hereafter SY98; Papovich, Dickinson, & Ferguson 2001, hereafter P01; Shapley et al. 2001). Independent measures of their kinematic masses, metallicities, SFRs, and initial mass functions (IMFs) have been determined using rest-frame UV and optical spectroscopy (Pettini et al. 2000, 2001, 2002; Shapley et al. 2001; Erb et al. 2003).

Despite these advances, it has proved difficult to reconcile the ages, SFRs, and stellar masses of individual galaxies at

[1] Based on observations with the NASA/ESA *Hubble Space Telescope*, obtained at the Space Telescope Science Institute, which is operated by the the Association of Universities for Research in Astronomy (AURA), Inc., under NASA contract NAS5-26555. Also based on observations collected at the European Southern Observatories on Paranal, Chile as part of the ESO program 164.O-0612.

[2] Max-Planck-Institut für Astrophysik, Karl-Schwarzschild-Strasse 1, Garching D-85741, Germany; grudnick@mpa-garching.mpg.de.

[3] Max-Planck-Institut für Astronomie, Königstuhl 17, Heidelberg D-69117, Germany.

[4] Leiden Observatory, P.O. Box 9513, 2300 RA Leiden, Netherlands.

[5] Department of Physics, New York University, 4 Washington Place, New York, NY 10003.

[6] European Southern Observatory, Karl-Schwarzschild-Strasse 2, Garching D-85748, Germany.

[7] Astronomy Department, Yale University, P.O. Box 208101, New Haven, CT 06520-8101.

different redshifts within a single galaxy formation scenario. Low-redshift studies of the fundamental plane indicate that the stars in elliptical galaxies must have been formed by $z > 2$ (e.g., van Dokkum et al. 2001), and observations of evolved galaxies at $1 < z < 2$ indicate that the present population of elliptical galaxies was already in place at $z \gtrsim 2.5$ (e.g., Benítez et al. 1999; Cimatti et al. 2002; but see Zepf 1997). In contrast, studies of star-forming LBGs spectroscopically confirmed to lie at $z > 2$ (Steidel et al. 1996, 1999) claim that LBGs are uniformly very young and a factor of 10 less massive than present-day L_* galaxies (e.g., SY98; P01; Shapley et al. 2001).

An alternative method of tracking the buildup of the cosmic stellar mass is to measure the total emissivity of all relatively unobscured stars in the universe, thus effectively making a luminosity-weighted mean of the galaxy population. This can be partly accomplished by measuring the evolution in the global luminosity density $j(z)$ from galaxy redshift surveys. Early studies at intermediate redshift have shown that the rest-frame UV and B-band $j(z)$ are steeply increasing out to $z \sim 1$ (e.g., Lilly et al. 1996; Fried et al. 2001). Wolf et al. (2003) have recently measured $j(z)$ at $0 < z < 1.2$ from the COMBO-17 survey, using $\sim$25,000 galaxies with redshifts accurate to $\sim$0.03 and a total area of 0.78 deg^2. At rest-frame 2800 Å, these measurements confirm those of Lilly et al. (1996) but do not support claims for a shallower increase with redshift, which goes as $(1+z)^{1.5}$, as claimed by Cowie, Songaila, & Barger (1999) and Wilson et al. (2002). On the other hand, the B-band evolution from Wolf et al. (2003) is only a factor of $\sim$1.6 between $0 < z < 1$, considerably shallower than the factor of $\sim$3.75 increase seen by Lilly et al. (1996). At $z > 2$, measurements of the rest-frame UV $j(z)$ have been made using the optically selected LBG samples (e.g., Madau et al. 1996; Sawicki, Lin, & Yee 1997; Steidel et al. 1999; Poli et al. 2001) and NIR-selected samples (Kashikawa et al. 2003; Poli et al. 2003; Thompson 2003), and, with modest extinction corrections, the most recent estimates generically yield rest-frame UV $j(z)$ curves that, at $z > 2$, are approximately flat out to $z \sim 6$ (cf. Lanzetta et al. 2002). Dickinson et al. (2003, hereafter D03) have used deep NIR data from NICMOS in the Hubble Deep Field–North (HDF-N) to measure the rest-frame B-band luminosity density out to $z \sim 3$, finding that it remained constant to within a factor of $\sim$3. By combining $j(z)$ measurements at different rest-frame wavelengths and redshifts, Madau, Pozzetti, & Dickinson (1998) and Pei, Fall, & Hauser (1999) modeled the emission in all bands, using an assumed global star formation history (SFH), and used it to constrain the mean extinction, metallicity, and IMF. Bolzonella, Pelló, & Maccagni (2002) measured NIR luminosity functions in the HDF-N and HDF-S and found little evolution in the bright end of the galaxy population and no decline in the rest-frame NIR luminosity density out to $z \sim 2$. In addition, Baldry et al. (2002) and Glazebrook et al. (2003) have used the mean optical cosmic spectrum at $z \sim 0$ from the 2dFGRS and the SDSS, respectively, to constrain the cosmic SFH.

Despite the wealth of information obtained from studies of the integrated galaxy population, there are major difficulties in using these many disparate measurements to reconstruct the evolution in the stellar mass density. First, and perhaps most important, the selection criteria for the low- and high-redshift surveys are usually vastly different. At $z < 1$ galaxies are selected by their rest-frame optical light. At $z > 2$, however, the dearth of deep, wide-field NIR imaging has forced galaxy selection by the rest-frame UV light. Observations in the rest-frame UV are much more sensitive to the presence of young stars and extinction than observations in the rest-frame optical. Second, state-of-the-art deep surveys have only been performed in small fields and the effects of field-to-field variance at faint magnitudes and in the rest-frame optical are not well understood.

In the face of field-to-field variance, the globally averaged rest-frame color may be a more robust characterization of the galaxy population than either the luminosity density or the mass density, because it is, to the first order, insensitive to the exact density normalization. At the same time, it encodes information about the dust obscuration, metallicity, and SFH of the cosmic stellar population. It therefore provides an important constraint on galaxy formation models that may be reliably determined from relatively small fields.

To track consistently the globally averaged evolution of the galaxies that dominate the stellar mass budget of the universe—as opposed to the UV luminosity budget—over a large redshift range, a strategy different from UV selection must be adopted. It is not only desirable to measure $j(z)$ in a constant rest-frame optical bandpass, but it is also necessary that galaxies be selected by light redward of the Balmer/4000 Å break, where the light from older stars contributes significantly to the spectral energy distribution (SED). To accomplish this, we obtained ultradeep NIR imaging of the WFPC2 field of the HDF-S (Casertano et al. 2000) with the Infrared Spectrograph and Array Camera (ISAAC; Moorwood 1997) at the Very Large Telescope (VLT) as part of the Faint Infrared Extragalactic Survey (FIRES; Franx et al. 2000). The FIRES data on the HDF-S, detailed in Labbé et al. (2003; hereafter L03), provide us with the deepest ground-based J_s and H data and the overall deepest K_s-band data in any field, allowing us to reach rest-frame optical luminosities in the V band of $\sim 0.6 L_*^{\rm local}$ at $z \sim 3$. First results, using a smaller set of the data, were presented in Rudnick et al. (2001; hereafter R01). The second FIRES field, centered on the $z = 0.83$ cluster MS 1054-03, has $\sim$1 mag less depth but $\sim$5 times greater area (N. M. Förster Schreiber et al. 2003, in preparation).

In the present work we draw on photometric redshift estimates, $z_{\rm phot}$, for the K_s band–selected sample in the HDF-S (R01; L03) and on the observed SEDs to derive rest-frame optical luminosities $L_\lambda^{\rm rest}$ for a sample of galaxies selected by light redder than the rest-frame V band out to $z \sim 3$. In § 2, we describe the observations, data reduction, and the construction of a K_s band–selected catalog with 0.3–2.2 μm photometry, which selects galaxies at $z < 4$ by light redward of the 4000 Å break. In § 3, we describe our photometric redshift technique, how we estimate the associated uncertainties in $z_{\rm phot}$, and how we measure $L_\lambda^{\rm rest}$ for our galaxies. In § 4, we use our measures of $L_\lambda^{\rm rest}$ for the individual galaxies to derive the mean cosmic luminosity density, $j_\lambda^{\rm rest}$, and the cosmic color and then use these to measure the stellar mass density, ρ_*, as a function of cosmic time. We discuss our results in § 5 and summarize in § 6. Throughout this paper we assume $\Omega_M = 0.3$, $\Omega_\Lambda = 0.7$, and $H_0 = 70\ h_{70}$ km s^{-1} Mpc^{-1}, unless explicitly stated otherwise.

2. DATA

A complete description of the FIRES observations, reduction procedures, and the construction of photometric

catalogs is presented in detail in L03; we outline the important steps below.

Objects were detected in the K_s-band image with version 2.2.2 of the SExtractor software (Bertin & Arnouts 1996). For consistent photometry between the space- and ground-based data, all images were then convolved to 0″.48, the worst seeing in our NIR bands. Photometry was then performed in the U_{300}-, B_{450}-, V_{606}-, I_{814}-, J_s-, H-, and K_s-band images using specially tailored isophotal apertures defined from the detection image. In addition, a measurement of the total flux in the K_s band, $K_{s,\mathrm{AB}}^{\mathrm{tot}}$, was obtained using an aperture based on the SExtractor *AUTO* aperture.[8] Our effective area is 4.74 arcmin^2, including only areas of the chip that were well exposed. All magnitudes are quoted in the Vega system unless specifically noted otherwise. Our adopted conversions from the Vega system to the AB system are $J_{s,\mathrm{Vega}} = J_{s,\mathrm{AB}} - 0.90$, $H_{\mathrm{Vega}} = H_{\mathrm{AB}} - 1.38$, and $K_{s,\mathrm{Vega}} = K_{s,\mathrm{AB}} - 1.86$ (Bessell & Brett 1988).

3. MEASURING PHOTOMETRIC REDSHIFTS AND REST-FRAME LUMINOSITIES

3.1. *Photometric Redshift Technique*

We estimated z_{phot} from the broadband SED, using the method described in R01, which attempts to fit the observed SED with a linear combination of redshifted galaxy templates. We made two modifications to the R01 method. First, we added an additional template constructed from a 10 Myr old, single-age, solar-metallicity population with a Salpeter (1955) IMF based on empirical stellar spectra from the 1999 version of the Bruzual A. & Charlot (1993) stellar population synthesis code. Second, a 5% minimum flux error was adopted for all bands to account for the night-to-night uncertainty in the derived zero points and for template mismatch effects, although in reality both of these errors are non-Gaussian.

Using 39 galaxies with reliable FIRES photometry and spectroscopy available from Cristiani et al. (2000), Rigopoulou et al. (2000), K. Glazebrook et al. (2003, in preparation),[9] Vanzella et al. (2002), and G. Rudnick et al. (2003, in preparation), we measured the redshift accuracy of our technique to be $\langle |z_{\mathrm{spec}} - z_{\mathrm{phot}}|/(1 + z_{\mathrm{spec}})\rangle = 0.09$ for $z < 3$. There is one galaxy at $z_{\mathrm{spec}} = 2.025$ with $z_{\mathrm{phot}} = 0.12$ but with a very large internal z_{phot} uncertainty. When this object is removed, $\langle |z_{\mathrm{spec}} - z_{\mathrm{phot}}|/(1 + z_{\mathrm{spec}})\rangle = 0.05$ at $z_{\mathrm{spec}} > 1.3$.

For a given galaxy, the photometric redshift probability distribution can be highly non-Gaussian and contain multiple χ^2 minima at vastly different redshifts. An accurate estimate of the error in z_{phot} must therefore not only contain the two-sided confidence interval in the local χ^2 minimum but also reflect the presence of alternate redshift solutions. The difficulties of measuring the uncertainty in z_{phot} were discussed in R01 and are not repeated in detail here. To improve on R01, however, we have developed a Monte Carlo method that takes into account, on a galaxy-by-galaxy basis, flux errors and template mismatch. These uncertainty estimates are called δz_{phot}. For a full discussion of this method, see Appendix A.

Galaxies with $K_{s,\mathrm{AB}}^{\mathrm{tot}} \geq 25$ have such high photometric errors that the z_{phot} estimates can be very uncertain. At $K_{s,\mathrm{AB}}^{\mathrm{tot}} < 25$, however, objects are detected at better than the 10 σ level and have well-measured NIR SEDs, important for locating redshifted optical breaks. For this reason, we limited our catalog to the 329 objects that have $K_{s,\mathrm{AB}}^{\mathrm{tot}} < 25$, lie on well-exposed sections of the chip, and are not identified as stars (see § 3.1.1).

3.1.1. *Star Identification*

To identify probable stars in our catalog, we did not use the profiles measured from the WFPC2 imaging, because it is difficult to determine the size at faint levels. At the same time, we verified that the stellar template fitting technique described below identified all bright, unsaturated stars in the image. Instead, we compared the observed SEDs with those from 135 NextGen, version 5.0, stellar atmosphere models described in Hauschildt, Allard, & Baron (1999).[10] We used models with $\log g$ of 5.5 and 6, effective temperatures ranging from 1600 to 10,000 K, and metallicities of solar and 1/10 solar. We identified an object as a stellar candidate if the raw χ^2 of the stellar fit was lower than that of the best-fit galaxy template combination. Four of the stellar candidates from this technique (objects 155, 230, 296, and 323) are obviously extended and were excluded from the list of stellar candidates. Two bright stars (objects 39 and 51) were not identified by this technique because they are saturated in the *HST* images and were added to the list by hand. We ended up with a list of 29 stars that have $K_{s,\mathrm{AB}}^{\mathrm{tot}} < 25$ and lie on well-exposed sections of the chip. These were excluded from all further analysis.

3.2. *Rest-Frame Luminosities*

To measure the $L_\lambda^{\mathrm{rest}}$ of a galaxy, one must combine its redshift with the observed SED to estimate the intrinsic SED. In practice, this requires some assumptions about the intrinsic SED.

In R01 we derived rest-frame luminosities from the best-fit combination of spectral templates at z_{phot}, which assumes that the intrinsic SED is well modeled by our template set. We know that for many galaxies the best-fit template matches the position and strength of the spectral breaks and the general shape of the SED. There are, however, galaxies in our sample that show clear residuals from the best-fit template combination. Even for the qualitatively good fits, the model and observed flux points can differ by ~10%, corresponding to a ~15% error in the derived rest-frame color. As we see in § 4.2, such color errors can cause errors of up to a factor of 1.5 in the V-band stellar mass-to-light ratio, M/L_V^*.

Here we used a method of estimating $L_\lambda^{\mathrm{rest}}$ that does not depend directly on template fits to the data but rather interpolates directly between the observed bands, using the templates as a guide. We define our rest-frame photometric system in Appendix B and explain our method for estimating $L_\lambda^{\mathrm{rest}}$ in Appendix C.

We plot in Figure 1 the rest-frame luminosities versus redshift and enclosed volume for the $K_{s,\mathrm{AB}}^{\mathrm{tot}} < 25$ galaxies in the FIRES sample. The different symbols represent different δz_{phot} values, and since the derived luminosity is tightly

[8] The reduced images, photometric catalogs, photometric redshift estimates, and rest-frame luminosities are available online through the FIRES home page at http://www.strw.leidenuniv.nl/~fires.

[9] Catalogs are available at http://www.aao.gov.au/hdfs.

[10] Available at http://dilbert.physast.uga.edu/~yeti/mdwarfs.html.

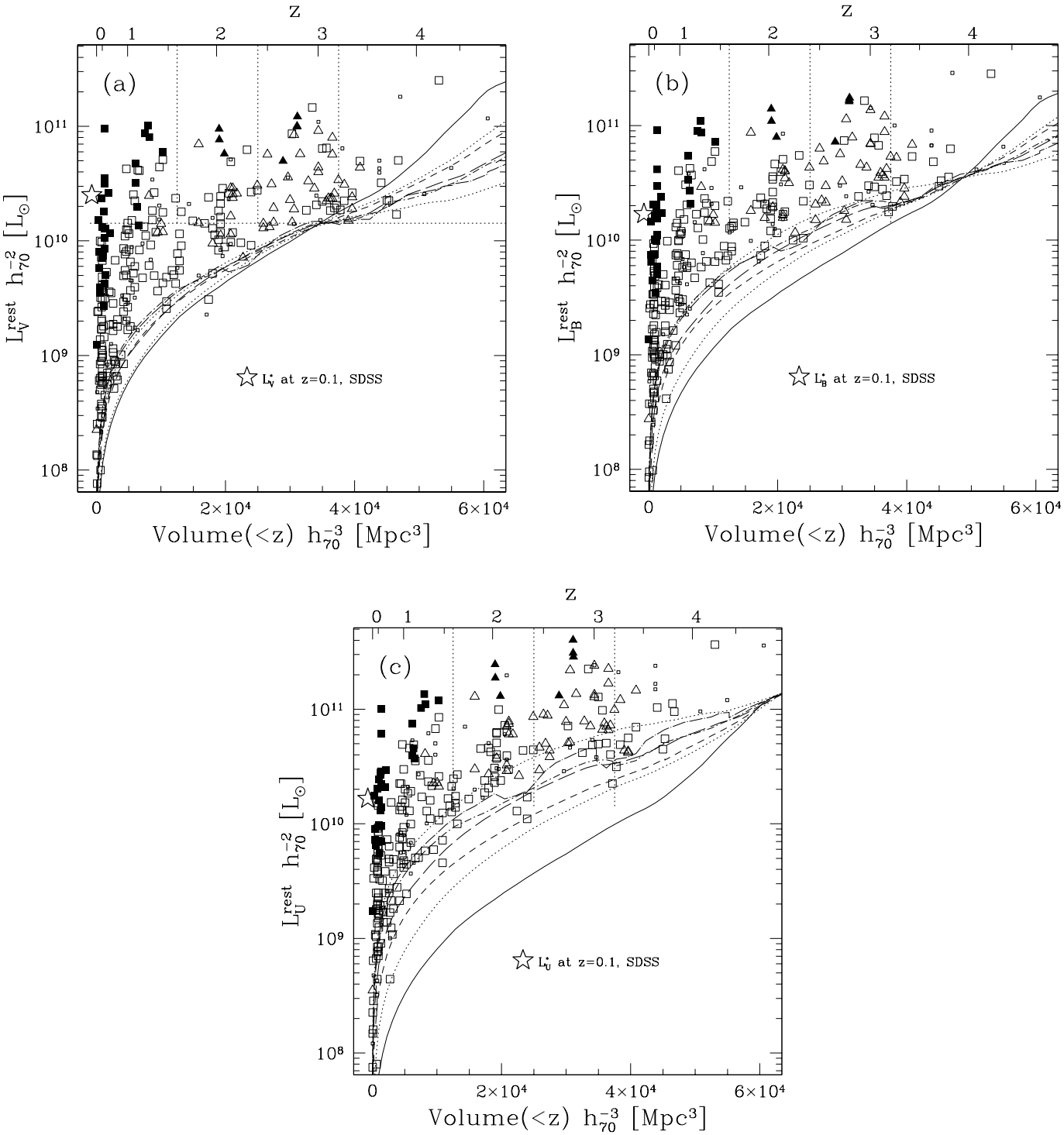

FIG. 1.—Distribution of rest-frame luminosities as a function of enclosed comoving volume and z, for galaxies with $K_{s,\mathrm{AB}}^{\mathrm{tot}} < 25$: (*a*) V band; (*b*) B band; (*c*) U band. Galaxies that have spectroscopic redshifts are represented by filled points, and for these objects $L_\lambda^{\mathrm{rest}}$ is measured at z_{spec}. Large symbols have $\delta z_{\mathrm{phot}}/(1+z_{\mathrm{phot}}) < 0.16$, and small symbols have $\delta z_{\mathrm{phot}}/(1+z_{\mathrm{phot}}) \geq 0.16$. Triangles are for objects classified as U-dropouts according to the selection of Giavalisco & Dickinson (2001). As is expected, most of the galaxies selected as U-dropouts have $z \gtrsim 2$. Note, however, the large numbers of rest-frame optically luminous galaxies at $z > 2$, which would not be selected as U-dropouts. The large stars in each panel indicate the value of L_*^{local} from B03. In the V band we are sensitive to galaxies at 60% of L_*^{local}, even at $z \sim 3$, and there are galaxies at $z_{\mathrm{phot}} \geq 2$ with $L_\lambda^{\mathrm{rest}} \geq 10^{11}\ \mathrm{h}_{70}^{-2}\ L_\odot$. The tracks represent the values of $L_\lambda^{\mathrm{rest}}$ for our seven template spectra, normalized at each redshift to $K_{s,\mathrm{AB}}^{\mathrm{tot}} = 25$. The specific tracks correspond to the E (*solid curve*), Sbc (*thick dotted curve*), Scd (*short-dashed curve*), Im (*long-dashed curve*), SB1 (*dot–short-dashed curve*), SB2 (*dot–long-dashed curve*), and 10my (*thin dotted curve*) templates. The horizontal dotted line in (*a*) indicates the luminosity threshold L_V^{thresh} above which we measure the rest-frame luminosity density $j_\lambda^{\mathrm{rest}}$, and the vertical dotted lines in each panel mark the redshift boundaries of the regions for which we measure $j_\lambda^{\mathrm{rest}}$. [*See the electronic edition of the Journal for a color version of this figure.*]

coupled to the redshift, we do not independently plot $L_\lambda^{\rm rest}$ error bars. The tracks indicate the $L_\lambda^{\rm rest}$ for different SED types, normalized to $K_{s,\rm AB}^{\rm tot} = 25$, while the intersection of the tracks in each panel indicates the redshift at which the rest-frame filter passes through our K_s-band detection filter. There is a wide range in $L_\lambda^{\rm rest}$ at all redshifts, and there are galaxies at $z > 2$ with $L_\lambda^{\rm rest}$ much in excess of the local L_* values. Using the full FIRES data set, we achieve much greater sensitivity than in R01; objects at $z \approx 3$ with $K_{s,\rm AB}^{\rm tot} = 25$ have $L_V^{\rm rest} \approx 0.6 * L_{*,V}^{\rm local}$, as defined from the $z = 0.1$ sample of B03. As seen in R01, there are many galaxies at $z > 2$, in all bands, with $L_\lambda^{\rm rest} \geq L_*^{\rm local}$. R01 found 10 galaxies at $2 \leq z \leq 3.5$ with $L_B^{\rm rest} > 10^{11}\ h_{70}^{-2}\ L_\odot$ and inferred a brightening in the luminosity function of ~1–1.3 mag. We confirm their result when using the same local luminosity function (Blanton et al. 2001). Although this brightening is biased upward by photometric redshift errors, we find a similar brightening of ~1 mag after correction for this effect. As also noted in R01, we found a deficit of luminous galaxies at $1.5 \lesssim z \lesssim 2$, although this deficit is not as pronounced at lower values of $L_\lambda^{\rm rest}$. The photometric redshifts in the HDF-S, however, are not well tested in this regime. To help judge the reality of this deficit, we compared our photometric redshifts on an object-by-object basis to those of the Rome group (Fontana et al. 2000),[11] who derived $z_{\rm phot}$ estimates for galaxies in the HDF-S using much shallower NIR data. We find generally good agreement in the $z_{\rm phot}$ estimates, although there is a large scatter at $1.5 < z < 2.0$. Both sets of photometric redshifts show a deficit in the $z_{\rm phot}$ distribution, although the Rome group's gap is less pronounced than ours and is at a slightly lower redshift. In addition, we examined the photometric redshift distribution of the NIR-selected galaxies of D03 in the HDF-N, which have very deep NIR data. These galaxies also showed a gap in the $z_{\rm phot}$ distribution at $z \sim 1.6$. Together, these results indicate that systematic effects in the $z_{\rm phot}$ determinations may be significant at $1.5 < z < 2.0$. On the other hand, we also derived photometric redshifts for a preliminary set of data in the MS 1054-03 field of the FIRES survey, whose filter set is similar, but which has a U instead of a U_{300} filter. In this field, no systematic depletion of $1.5 < z < 2$ galaxies was found. It is therefore not clear what role systematic effects play in comparison to field-to-field variations in the true redshift distribution over this redshift range. Obtaining spectroscopic redshifts at $1.5 < z < 2$ is the only way to judge the accuracy of the $z_{\rm phot}$ estimates in this regime.

We have also split the points up according to whether or not they satisfied the U-dropout criteria of Giavalisco & Dickinson (2001), which were designed to pick unobscured star-forming galaxies at $z \gtrsim 2$. As expected from the high efficiency of the U-dropout technique, we find that only 15% of the 57 classified U-dropouts have $z < 2$. As we discuss in § 4.1, we measured the luminosity density for objects with $L_V^{\rm rest} > 1.4 \times 10^{10}\ h_{70}^{-2}\ L_\odot$. Above this threshold, there are 62 galaxies with $2 < z < 3.2$, of which 26 are not classified as U-dropouts. These non–U-dropouts number among the most rest-frame optically luminous galaxies in our sample. In fact, the most rest-frame optically luminous object at $z < 3.2$ (object 611) is a galaxy that fails the U-dropout criteria. Ten of these 26 objects, including object 611, also have $(J-K) > 2.3$, a color threshold that has been shown by Franx et al. (2003) and van Dokkum et al. (2003) to efficiently select galaxies at $z > 2$. These galaxies are not only luminous but also have red rest-frame optical colors, implying high M/L^* values. Franx et al. (2003) showed that they likely contribute significantly (~43%) to the stellar mass budget at high redshifts.

[11] Available at http://www.mporzio.astro.it/HIGHZ/HDF.html.

3.2.1. *Emission Lines*

There will be emission-line contamination of the rest-frame broadband luminosities when rest-frame optical emission lines contribute significantly to the flux in our observed filters. P01 estimated the effect of emission lines in the NICMOS F160W filter and the K_s filter and found that redshifted, rest-frame optical emission lines, whose equivalent widths are at the maximum end of those observed for starburst galaxies (rest-frame equivalent width ~ 200 Å), can contribute up to 0.2 mag in the NIR filters. In addition, models of emission lines from Charlot & Longhetti (2001) show that emission lines will tend to drive the $(U-B)_{\rm rest}$ color to the blue more easily than the $(B-V)_{\rm rest}$ color for a large range of models. Using the UBV photometry and spectra of nearby galaxies from the Nearby Field Galaxy Survey (NFGS; Jansen et al. 2000a, 2000b), we computed the actual correction to the $(U-B)_{\rm rest}$ and $(B-V)_{\rm rest}$ colors as a function of $(B-V)_{\rm rest}$. For the bluest galaxies in $(B-V)_{\rm rest}$, emission lines bluen the $(U-B)_{\rm rest}$ colors by ~0.05 and the $(B-V)_{\rm rest}$ colors only by less than 0.01. Without knowing beforehand the strength of emission lines in any of our galaxies, we corrected our rest-frame colors based on the results from Jansen et al. We ignored the very small correction to the $(B-V)_{\rm rest}$ colors and corrected the $(U-B)_{\rm rest}$ colors using the equation

$$(U-B)_{\rm corrected} = (U-B) - 0.0658(B-V) + 0.0656\ , \quad (1)$$

which corresponds to a linear fit to the NFGS data. These effects might be greater for objects with strong AGN contribution to their fluxes.

4. THE PROPERTIES OF THE MASSIVE GALAXY POPULATION

In this section we discuss the use of the $z_{\rm phot}$ and $L_\lambda^{\rm rest}$ estimates to derive the integrated properties of the population, namely, the luminosity density, the mean cosmic rest-frame color, the stellar mass-to-light ratio M/L^*, and the stellar mass density ρ_*. As is described below, addressing the integrated properties of the population reduces many of the uncertainties associated with modeling individual galaxies and, in the case of the cosmic color, is less sensitive to field-to-field variations.

4.1. *The Luminosity Density*

Using our $L_\lambda^{\rm rest}$ estimates from the $K_{s,\rm AB}^{\rm tot} < 25$ galaxies (see § 3.2), we traced the redshift evolution of the rest-frame optically most luminous, and therefore presumably most massive, galaxies by measuring the rest-frame luminosity density $j_\lambda^{\rm rest}$ of the visible stars associated with them. The results are presented in Table 1 and plotted against redshift and elapsed cosmic time in Figure 2. As our best alternative to a selection by galaxy mass, we selected our galaxies in our reddest rest-frame band available at $z \sim 3$, i.e., the V band. In choosing the z and $L_\lambda^{\rm rest}$ regime over which we measured $j_\lambda^{\rm rest}$, we wanted to push to as high a redshift as possible, with

TABLE 1

Rest-Frame Optical Luminosity Density and Integrated Color

Survey	z	$\log j_U^{\rm rest}$ ($h_{70}\,L_{\odot,U}\,{\rm Mpc}^{-3}$)	$\log j_B^{\rm rest}$ ($h_{70}\,L_{\odot,B}\,{\rm Mpc}^{-3}$)	$\log j_V^{\rm rest}$ ($h_{70}\,L_{\odot,V}\,{\rm Mpc}^{-3}$)	$(U-B)_{\rm rest}$	$(B-V)_{\rm rest}$
SDSS	0.10 ± 0.10	$7.89^{+0.04}_{-0.05}$	$7.87^{+0.04}_{-0.05}$	$7.91^{+0.04}_{-0.05}$	0.14 ± 0.02	0.75 ± 0.02
COMBO-17	0.30 ± 0.10	7.84 ± 0.05	7.85 ± 0.05	7.93 ± 0.05	0.21 ± 0.02	0.84 ± 0.01
	0.50 ± 0.10	$8.01^{+0.04}_{-0.05}$	$7.99^{+0.04}_{-0.05}$	$8.01^{+0.04}_{-0.05}$	0.16 ± 0.01	$0.69^{+0.005}_{-0.01}$
	0.70 ± 0.10	$8.18^{+0.04}_{-0.05}$	$8.13^{+0.04}_{-0.05}$	$8.12^{+0.04}_{-0.05}$	0.06 ± 0.01	0.64 ± 0.01
	0.90 ± 0.10	$8.22^{+0.04}_{-0.05}$	$8.13^{+0.04}_{-0.05}$	$8.09^{+0.04}_{-0.05}$	$-0.04^{+0.004}_{-0.01}$	$0.55^{+0.005}_{-0.01}$
FIRES	$1.12^{+0.48}_{-1.12}$	$8.12^{+0.08}_{-0.09}$	8.02 ± 0.08	$8.01^{+0.08}_{-0.09}$	-0.04 ± 0.03	0.61 ± 0.02
	$2.01^{+0.40}_{-0.41}$	$8.22^{+0.08}_{-0.10}$	$8.00^{+0.08}_{-0.10}$	$7.90^{+0.08}_{-0.09}$	$-0.34^{+0.04}_{-0.03}$	0.38 ± 0.04
	$2.80^{+0.40}_{-0.39}$	$8.58^{+0.07}_{-0.08}$	$8.33^{+0.07}_{-0.08}$	$8.19^{+0.07}_{-0.08}$	$-0.44^{+0.04}_{-0.03}$	$0.29^{+0.04}_{-0.03}$

Note.—The quantity $j_\lambda^{\rm rest}$ and rest-frame colors are calculated for galaxies with $L_V^{\rm rest} > 1.4 \times 10^{10}\ h_{70}^{-2}\ L_{\odot,V}$.

the double constraint that the redshifted rest-frame filter still overlapped with the K_s filter and that we were equally complete at all considered redshifts. By choosing an $L_V^{\rm rest}$ threshold, $L_V^{\rm thresh} = 1.4 \times 10^{10}\ h_{70}^{-2}\ L_\odot$, and a maximum redshift of $z = 3.2$, we could select galaxies down to $0.6 L_{*,V}^{\rm local}$ with constant efficiency, regardless of SED type. We then divided the range out to $z = 3.2$ into three bins of equal comoving volume, which correspond to the redshift intervals 0–1.6, 1.6–2.41, and 2.41–3.2.

In a given redshift interval, we estimated $j_\lambda^{\rm rest}$ directly from the data in two steps. We first added up all the luminosities of galaxies that satisfied our $L_V^{\rm thresh}$ criteria defined above and had $\delta z_{\rm phot}/(1 + z_{\rm phot}) \leq 0.16$, roughly twice the mean disagreement between $z_{\rm phot}$ and $z_{\rm spec}$ (see § 3.1). Galaxies rejected by our $\delta z_{\rm phot}$ cut but with $L_V^{\rm rest} > L_V^{\rm thresh}$, however, contribute to the total luminosity, although they are not included in this first estimate. Under the assumption that these galaxies are drawn from the same luminosity function as those that passed the $\delta z_{\rm phot}$ cut, we computed the total luminosity, including the light from the $n_{\rm acc}$ accepted galaxies and the light lost from the $n_{\rm rej}$ rejected galaxies, as

$$L_{\rm tot} = L_{\rm meas} \times \left(1 + \frac{n_{\rm rej}}{n_{\rm acc}}\right). \quad (2)$$

As a test of the underlying assumption of this correction, we performed a Kolmogorov-Smirnov (K-S) test on the distributions of K_s magnitudes for the rejected and accepted galaxies in each of our three volume bins. In all three redshift bins, the rejected galaxies have $K_{s,\rm AB}^{\rm tot}$ distributions that are consistent at the greater than 90% level with being drawn from the same magnitude distribution as the accepted galaxies. The total correction per volume bin ranges from 5% to 10% in every bin. Our results do not change if we omit those galaxies whose photometric redshift probability distribution indicates a secondary minimum in χ^2.

Uncertainties in the luminosity density were computed by bootstrapping from the $K_{s,\rm AB}^{\rm tot} < 25$ subsample. This method does not take cosmic variance into account, and the errors may therefore underestimate the true error, which includes field-to-field variance.

Redshift errors might affect the luminosity density in a systematic way, as they produce a large error in the measured luminosity. This, combined with a steep luminosity function, can bias the observed luminosities upward, especially at the bright end. This effect can be corrected for in a full determination of the luminosity function (e.g., Chen et al. 2003), but for our application we estimated the strength of this effect by Monte Carlo simulations. When we used the formal redshift errors, we obtained a very small bias (6%); if we increase the photometric redshift errors in the simulation to be minimally as large as $0.08(1 + z)$, we still obtain a bias in the luminosity density on the order of 10% or less.

Because we exclude galaxies with faint rest-frame luminosities or low apparent magnitudes and do not correct for this incompleteness, our estimates should be regarded as lower limits on the total luminosity density. One possibility for estimating the total luminosity density would be to fit a luminosity function as a function of redshift and then integrate it over the whole luminosity range. At high redshift, however, we do not probe far enough down the luminosity function to tightly constrain the faint-end slope α. Because extrapolation of $j_\lambda^{\rm rest}$ to arbitrarily low luminosities is very dependent on the value of α, we choose to use this simple and direct method instead. Including all galaxies with $K_{s,\rm AB}^{\rm tot} < 25$ raises the $j_\lambda^{\rm rest}$ values in the $z = 0$–1.6 redshift bin by 86%, 74%, and 66% in the U, B, and V bands, respectively. Likewise, the $j_\lambda^{\rm rest}$ values would increase by 38%, 35%, and 44% for the $z = 1.6$–2.41 bin and by 5%, 5%, and 2% for the $z = 2.41$–3.2 bin in the U, B, and V bands, respectively.

The dip in the luminosity density in the second-lowest redshift bin of Figures 2*a* and 2*b* can be traced to the lack of intrinsically luminous galaxies at $z \sim 1.5$–2 (§ 3.2; R01). The dip is not noticeable in the U band, because the galaxies at $z \sim 2$ are brighter with respect to the $z < 1.6$ galaxies in the U band than in the V or B bands; i.e., they have bluer $(U-B)_{\rm rest}$ colors and $(U-V)_{\rm rest}$ colors than galaxies at $z < 1.6$. This lack of rest-frame optically bright galaxies at $z \sim 1.5$–2 may result from systematics in the $z_{\rm phot}$ estimates, which are poorly tested in this regime and for which the Lyman break has not yet entered the U_{300} filter, or may reflect a true deficit in the redshift distribution of K_s-band luminous galaxies (see § 3.2).

At $z \lesssim 1$ our survey is limited by its small volume. For this reason, we supplement our data with other estimates of $j_\lambda^{\rm rest}$ at $z \lesssim 1$.

We compared our results with those of the SDSS as follows. First, we selected SDSS main-sample galaxies (Strauss et al. 2002) with redshifts in the SDSS Early Data Release (EDR; Stoughton et al. 2002) sample provided by and described by Blanton et al. (2003c). Using the product *kcorrect v1_16* (Blanton et al. 2003a), for each galaxy we fitted an optical SED to the ${}^{0.1}u^{0.1}g^{0.1}r^{0.1}i^{0.1}z$ magnitudes, after correcting the magnitudes to $z = 0.1$ for evolution using the results of B03. We projected this SED onto the *UBV* filters, as described by Bessell (1990), to obtain

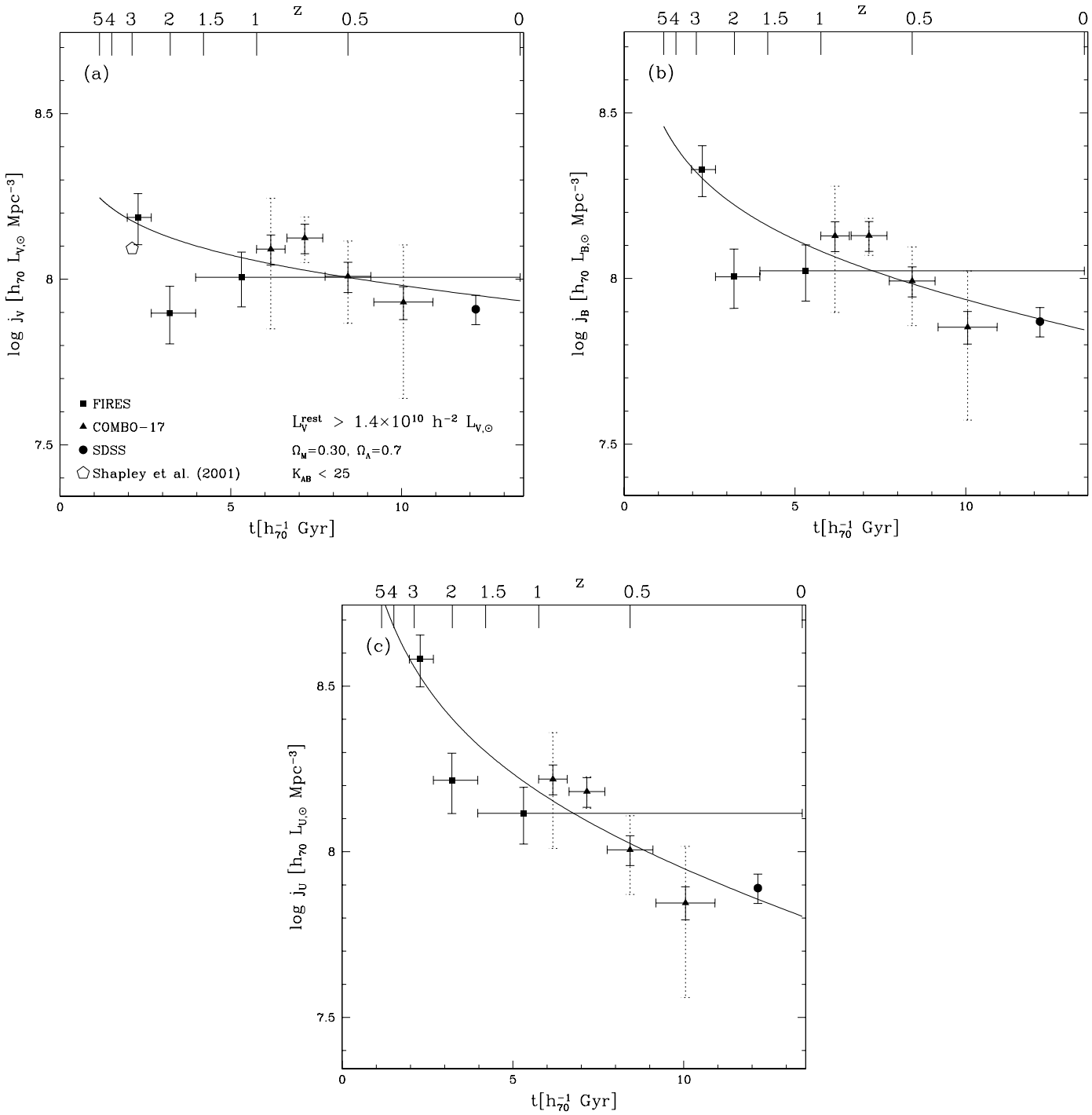

FIG. 2.—Rest-frame optical luminosity density vs. cosmic age and redshift from galaxies with $K_{s,\mathrm{AB}}^{\mathrm{tot}} < 25$ and $L_V^{\mathrm{rest}} > L_V^{\mathrm{thresh}}$: (*a*) V band; (*b*) B band; (*c*) U band. For comparison, we plot $j_\lambda^{\mathrm{rest}}$ determinations from other surveys down to our L_V^{rest} limits: from our data (*squares*), from the COMBO-17 survey (Wolf et al. 2003; *triangles*), at $z = 0.1$ from the SDSS (B03; *circle*), and from Shapley et al. (2001; *pentagon*). The dotted error bars on the COMBO-17 data indicate the rms field-to-field variation derived from the three spatially distinct COMBO-17 fields. The solid line represents a power-law fit to the FIRES, COMBO-17, and SDSS data of the form $j_\lambda^{\mathrm{rest}}(z) = j_\lambda^{\mathrm{rest}}(0)(1+z)^\beta$. [*See the electronic edition of the Journal for a color version of this figure.*]

absolute magnitudes in the *UBV* Vega relative system. Using the method described in Blanton et al. (2003c), we calculated the maximum volume $V_{\max}$ within the EDR over which each galaxy could have been observed, accounting for the survey completeness map and the flux limit as a function of position. The quantity $1/V_{\max}$ then represents the number density contribution of each galaxy. From these results we constructed the number density distribution of galaxies as a function of color and absolute magnitude and the contribution to the uncertainties in those densities from Poisson statistics. While the Poisson errors in the SDSS are negligible, cosmic variance does contribute to the uncertainties. For a more realistic error estimate, we use the fractional errors on the luminosity density from B03. For the SDSS luminosity function, our L_V^{thresh} encompasses 54% of the total light.

In Figure 2, we also show the $j_\lambda^{\rm rest}$ measurements from the COMBO-17 survey (Wolf et al. 2003). We used a catalog with updated redshifts and 29,471 galaxies at $z < 0.9$, of which 7441 had $L_V^{\rm rest} > L_V^{\rm thresh}$ (the J2003.0 catalog; C. Wolf 2003, private communication). Using this catalog, we calculated $j_\lambda^{\rm rest}$ in a way identical to how it was calculated for the FIRES data. We divided the data into redshift bins of $\Delta z = 0.2$ and counted the light from all galaxies contained within each bin that had $L_V^{\rm rest} > L_V^{\rm thresh}$. The formal 68% confidence limits were calculated via bootstrapping. In addition, in Figure 2 we indicate the rms field-to-field variations between the three spatially distinct COMBO-17 fields. As also pointed out in Wolf et al. (2003), the field-to-field variations dominate the error in the COMBO-17 $j_\lambda^{\rm rest}$ determinations.

Bell et al. (2003b) point out that uncertainties in the absolute and relative calibration of the SDSS and Johnson zero points can lead to $\lesssim$10% errors in the derived rest-frame magnitudes and colors of galaxies. To account for this, we add a 10% error in quadrature with the formal errors for both the COMBO-17 and SDSS luminosity densities. These are the errors presented in Table 1 and Figure 2.

In Figure 2*a*, we also plot the $j_V^{\rm rest}$ value of luminous LBGs determined by integrating the luminosity function of Shapley et al. (2001) to $L_V^{\rm thresh}$. A direct comparison between our sample and theirs is not entirely straightforward, because the LBGs represent a specific class of nonobscured, star-forming galaxies at high redshift, selected by their rest-frame far-UV light. Nonetheless, our $j_\lambda^{\rm rest}$ determination at $z = 2.8$ is slightly higher than their determination at $z = 3$, indicating either that the HDF-S is overdense with respect to the area surveyed by Shapley et al. or that we may have galaxies in our sample that are not present in the ground-based LBG sample.

D03 have also measured the luminosity density in the rest-frame *B* band, but because they do not give their luminosity function parameters, except for their lowest redshift bin, it is not possible to overplot their luminosity density integrated down to our $L_V^{\rm rest}$ limit.

4.1.1. *The Evolution of* $j_\lambda^{\rm rest}$

We find progressively stronger luminosity evolution from the *V* to the *U* band: whereas the evolution is quite weak in *V*, it is very strong in *U*. The $j_\lambda^{\rm rest}$ in our highest redshift bin is a factor of 1.9 ± 0.4, 2.9 ± 0.6, and 4.9 ± 1.0 higher than the $z = 0.1$ value in *V*, *B*, and *U*, respectively. To address the effect of cosmic variance on the measured evolution in $j_\lambda^{\rm rest}$, we rely on the clustering analysis developed for our sample in Daddi et al. (2003). Using the correlation length estimated at $2 < z < 4$, $r_0 = 5.5\ h_{100}^{-1}$ Mpc, we calculated the expected 1 σ fluctuations in the number density of objects in our two highest redshift bins. Because for our high-*z* samples the Poissonian errors are almost identical to the bootstrap errors, we can use the errors in the number density as a good proxy for the errors in $j_\lambda^{\rm rest}$. The inclusion of the effects of clustering would increase the bootstrap errors on the luminosity density by a factor of, at most, 1.75 downward and 2.8 upward. This implies that the inferred evolution is still robust even in the face of the measured clustering. The COMBO-17 data appear to have a slightly steeper rise toward higher redshift than our data; however, there are two effects to remember at this point. First, our lowest redshift point averages over all redshifts $z < 1.6$, in which case we are in reasonably good agreement with what one would predict from the average of the SDSS and COMBO-17 data. Second, our data may simply have an offset in density with respect to the local measurements. Such an offset affects the values of $j_\lambda^{\rm rest}$, but as we show in § 4.2, it does not strongly affect the global color estimates. Nonetheless, given the general increase with $j_\lambda^{\rm rest}$ toward higher redshifts, we fit the changing $j_\lambda^{\rm rest}$ with a power law of the form $j_\lambda^{\rm rest}(z) = j_\lambda^{\rm rest}(0)(1+z)^\beta$. These curves are overplotted in Figure 2, and the best-fit parameters in sets of $[j_\lambda^{\rm rest}(0), \beta]$ are $(5.96 \times 10^7, 1.41)$, $(6.84 \times 10^7, 0.93)$, and $(8.42 \times 10^7, 0.52)$ in the *U*, *B*, and *V* bands, respectively, where $j_\lambda^{\rm rest}(0)$ has units of $h_{70}\ L_\odot\ {\rm Mpc}^{-3}$. At the same time, it is important to remember that our power-law fit is likely an oversimplification of the true evolution in $j_\lambda^{\rm rest}$.

The increase in $j_\lambda^{\rm rest}$ with decreasing cosmic time can be modeled as a simple brightening of L_*. Performing a test similar to that performed in R01, we determine the increase in $L_{*,V}$ with respect to $L_{*,V}^{\rm local}$ needed to match the observed increase in $j_\lambda^{\rm rest}$ from $z = 0.1$ to $2.41 < z < 3.2$, assuming the SDSS Schechter function parameters. To convert between the Schechter function parameters in the SDSS bands and those in the Bessell (1990) filters, we transformed the $L_{*,{}^{0.1}r}^{\rm SDSS}$ values to the Bessell *V* filter using the $(V - {}^{0.1}r)$ color, where the color was derived from the total luminosity densities in the indicated bands (as given in B03). We then applied the appropriate AB-to-Vega correction tabulated in Bessell (1990). Because the difference in $\lambda_{\rm eff}$ is small between the two filters in each of these colors, the shifts between the systems are less than 5%. The luminosity density in the *V* band at $2.41 < z < 3.2$ is $j_V^{\rm rest} = (1.53 \pm 0.26) \times 10^8\ h_{70}\ L_\odot\ {\rm Mpc}^{-3}$. Using the *V*-band Schechter function parameters for our cosmology, $\phi_*^{\rm SDSS} = 5.11 \times 10^{-3}\ h_{70}^3\ {\rm Mpc}^{-3}$, $\alpha^{\rm SDSS} = -1.05$, and $L_{*,V}^{\rm SDSS} = 2.53 \times 10^{10}\ h_{70}^{-2}\ L_\odot$, we can match the increase in $j_V^{\rm rest}$ if $L_{*,V}$ brightens by a factor of 1.7 out to $2.41 < z < 3.2$.

4.2. *The Cosmic Color*

Using our measures of $j_\lambda^{\rm rest}$, we estimated the cosmic rest-frame color of all the visible stars that lie in galaxies with $L_V^{\rm rest} > 1.4 \times 10^{10}\ h_{70}^{-2}\ L_\odot$. We derived the mean cosmic $(U-B)_{\rm rest}$ and $(B-V)_{\rm rest}$ by using the $j_\lambda^{\rm rest}$ estimates from the previous section with the appropriate magnitude zero points. The measured colors for the FIRES, COMBO-17, and SDSS data are given in Table 1. Emission line–corrected $(U-B)_{\rm rest}$ colors may be calculated by applying equation (1) to the values in the table. For the FIRES and COMBO-17 data, uncertainty estimates are derived from the same bootstrapping simulation used in § 4.1. In this case, however, the COMBO-17 and SDSS error bars do not include an extra component from errors in the transformation to rest-frame luminosities, since these transformation errors may be correlated in a nontrivial way.

The bluing with increasing redshift, which could have been inferred from Figure 2, is seen explicitly in Figure 3. The color change toward higher redshift occurs more smoothly than the evolution in $j_\lambda^{\rm rest}$, with our FIRES data meshing nicely with the COMBO-17 data. It is immediately apparent that the rms field-to-field errors for the COMBO-17 data are much less than the observed trend in color, in contrast to Figure 2. This explicitly shows that the integrated color is much less sensitive than $j_\lambda^{\rm rest}$ to field-to-field variations, even when such variations may dominate the

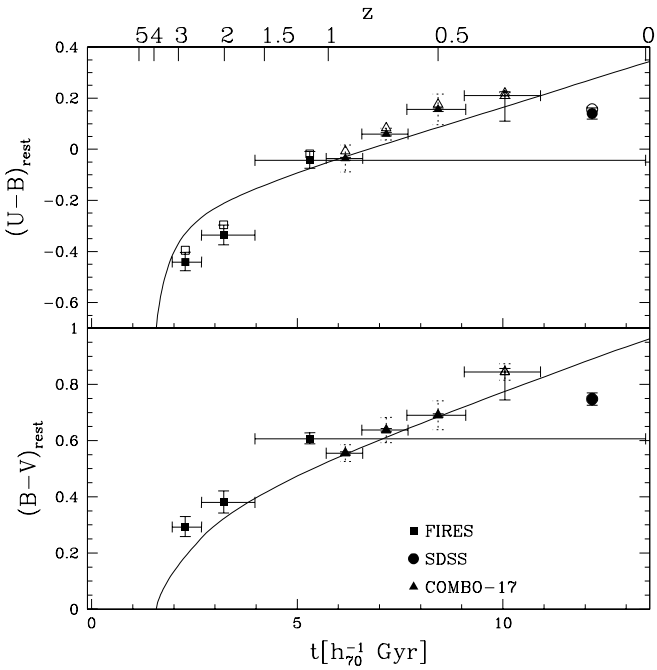

FIG. 3.—Evolution of the cosmic color vs. redshift and cosmic time for our data (*squares*), and those from other $z \lesssim 1$ surveys: COMBO-17 (Wolf et al. 2003; *triangles*) and SDSS (at $z = 0.1$; B03; *circle*). The open symbols indicate the empirical emission-line correction to the integrated colors, derived using the spectroscopic and photometric data from the NFGS (Jansen et al. 2000a). The dotted error bars on the COMBO-17 data indicate the field-to-field variation. Note that the integrated rest-frame color is much more stable than $j_\lambda^{\rm rest}$ against field-to-field variations. The COMBO-17 data point at $z = 0.3$ has been given a color error bar of 0.1 in the blueward direction and an open symbol to reflect the possible systematic biases resulting from their very small central apertures. We also overplot a model with an exponentially declining SFH with $\tau = 6$ Gyr, $E(B-V) = 0.35$, and $z_{\rm start} = 4.0$, assuming a Calzetti et al. (2000) extinction law. [*See the electronic edition of the Journal for a color version of this figure.*]

error in the luminosity density. The COMBO-17 data at $z \lesssim 0.4$ are also redder than the local SDSS data, possibly owing to the very small central apertures used to measure colors in the COMBO-17 survey. The colors in the COMBO-17 data were measured with the package MPIAPHOT using the peak surface brightness in images all smoothed to identical seeing (1″.5). Such small apertures were chosen to measure very precise colors, not to obtain global color estimates. Because of color gradients, these small apertures can overestimate the global colors in nearby well-resolved galaxies, while providing more accurate global color estimates for the more distant objects. Following the estimates of this bias provided by Bell et al. (2003b), we increased the color error bars on the blue side to 0.1 for the $z < 0.4$ COMBO-17 data. It is encouraging to see that the color evolution is roughly consistent with a rather simple model and that it is much smoother than the luminosity density evolution, which is more strongly affected by cosmic variance.

We interpreted the color evolution as being primarily driven by a decrease in the stellar age with increasing redshift. Applying the $(B-V)_{\rm rest}$–dependent emission-line corrections inferred from local samples (see § 3.2.1), we see that the effect of the emission lines on the color is much less than the magnitude of the observed trend. We can also interpret this change in color as a change in mean cosmic M/L^* with redshift. In this picture, which is true for a variety of monotonic SFHs and extinctions, the points at high redshift have lower M/L^*s than those at low redshift. At the same time, however, the evolution in $j_V^{\rm rest}$ with redshift is quite weak. Taken together, this would imply that the stellar mass density ρ_* is also decreasing with increasing redshift. We quantify this in § 4.3.

To show how our mean cosmic $(U-B)_{\rm rest}$ and $(B-V)_{\rm rest}$ colors compare to those of morphologically normal nearby galaxies, we overplot them in Figure 4 on the locus of nearby galaxies from Larson & Tinsley (1978). The integrated colors, at all redshifts, lie very close to the local track, which Larson & Tinsley (1978) demonstrated is easily reproducible with simple, monotonically declining SFHs and which is preserved in the presence of modest amounts of reddening, which moves galaxies roughly parallel to the locus. In fact, correcting our data for emission lines moved them even closer to the local track. While we have suggested that M/L^* decreases with decreasing color, if we wish to actually quantify the M/L^* evolution from our data we must first attempt to find a set of models that can match our observed colors. We then use these models to convert between the color and M/L_V^*. We overplot in Figure 4 three

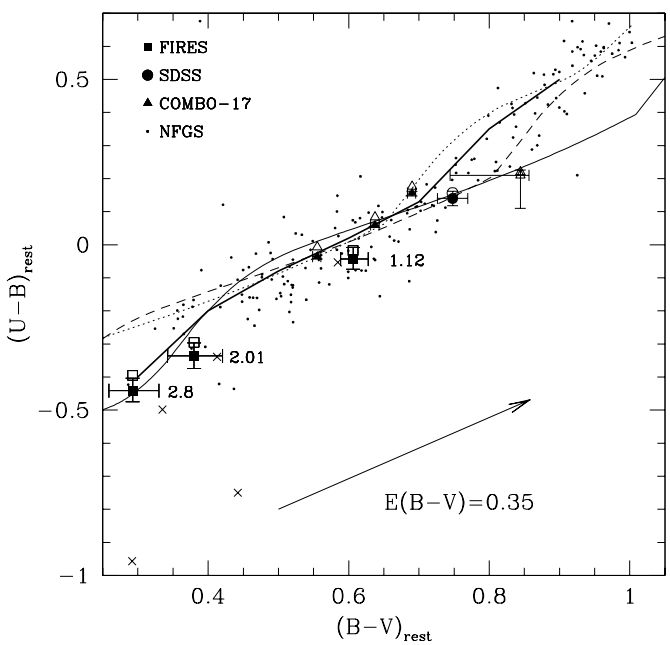

FIG. 4.—$(U-B)_{\rm rest}$ vs. $(B-V)_{\rm rest}$ at $z = 1.12$, 2.01, and 2.8 of all the relatively unobscured stars in galaxies with $L_V^{\rm rest} > 1.4 \times 10^{10}\ h_{70}^{-2}\ L_\odot$. The thick solid line represents the local relation derived by Larson & Tinsley (1978) from nearby morphologically normal galaxies. The large symbols are the same as in Fig. 3. For clarity we do not plot the field-to-field error bars for the COMBO-17 data. The small points are for the colors of nearby galaxies from the NFGS (Jansen et al. 2000b), which have been corrected for emission lines. The small crosses are for the NFGS galaxies that harbor AGNs. The thin tracks correspond to an exponentially declining SFH with a timescale of 6 Gyr. The tracks were created using a Salpeter (1955) IMF and the 2000 version of the Bruzual A. & Charlot (1993) models. The tracks have been reddened by $E(B-V) = 0$ (*dotted track*), $E(B-V) = 0.15$ (*dashed track*), and $E(B-V) = 0.35$ (*thin solid track*), using the Calzetti et al. (2000) extinction law. The arrow indicates the reddening vector applied to the solid-model track. The emission line–corrected data lie very close the track defined by observations of local galaxies, and the agreement with the models demonstrates that simple SFHs can be used to reproduce the integrated colors from massive galaxies at all redshifts. [*See the electronic edition of the Journal for a color version of this figure.*]

model tracks corresponding to an exponential SFH with $\tau = 6$ Gyr and $E(B-V) = 0$, 0.15, and 0.35 (assuming a Calzetti et al. 2000 reddening law). These tracks were calculated using the 2000 version of the Bruzual A. & Charlot (1993) models and have $Z = Z_\odot$ and a Salpeter (1955) IMF with a mass range of 0.1–120 $M_\odot$. Other exponentially declining models, and even a constant star-forming track, all yield colors similar to those of the $\tau = 6$ Gyr track. The measured cosmic colors at $z < 1.6$ are fairly well approximated by either of the reddened models. At $z > 1.6$, however, only the $E(B-V) = 0.35$ track can reproduce the data. This high extinction is in contrast to the results of P01 and Shapley et al. (2001), who found a mean reddening for LBGs of $E(B-V) \sim 0.15$. SY98 and Thompson, Weymann, & Storrie-Lombardi (2001), however, measured extinctions on this order for galaxies in the HDF-N, although the mean extinction from Thompson et al. (2001) was lower at $z > 2$. The amount of reddening in our sample is one of the largest uncertainties in deriving the M/L^* values; nonetheless, our choice of a high extinction is the only allowable possibility, given the integrated colors of our high-redshift data.

Although this figure demonstrates that the measured colors can be matched, at some age, by this simple $E(B-V) = 0.35$ model, we must nevertheless investigate whether the evolution of our model colors is also compatible with the evolution in the measured colors. This is shown by the track in Figure 3. We have tried different combinations of τ, $E(B-V)$, and $z_{\rm start}$, but we have not been able to find a model that fits the data well at all redshifts. The parameterized SFR(z) curve of Cole et al. (2001) also provided a poor fit to the data. Given the large range of possible parameters, our data may not be sufficient to well constrain the SFH.

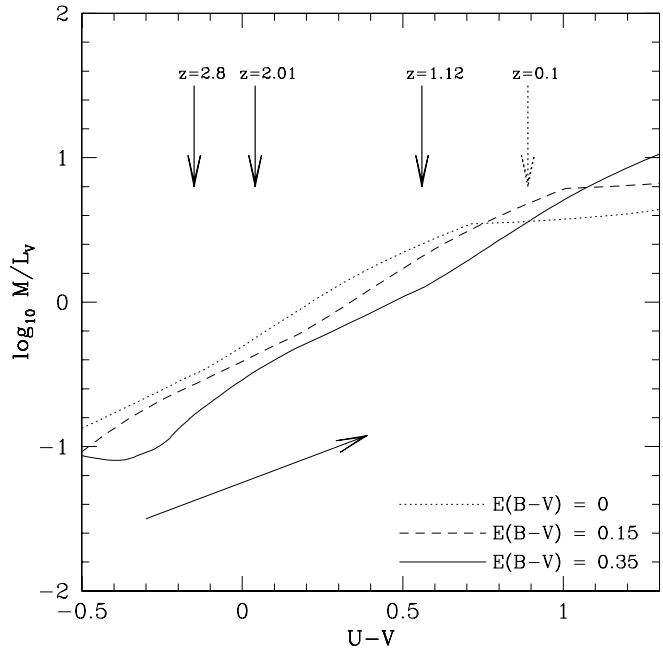

FIG. 5.—Relation between $(U-V)$ and M/L_V^* for a model track with an exponential timescale of 6 Gyr. The dotted line is for a model with $E(B-V) = 0$, the dashed line for a model with $E(B-V) = 0.15$, and the solid line for a model with $E(B-V) = 0.35$ (using a Calzetti extinction law), which we adopt for our M/L_V^* conversions. The vertical solid arrows indicate the colors of the three FIRES data points, the vertical dotted arrow indicates the color of the SDSS data, and the diagonal arrow indicates the vector used to redden the $E(B-V) = 0$ model to $E(B-V) = 0.35$. The labels above the vertical arrows correspond to the redshifts of the FIRES and SDSS data. [*See the electronic edition of the Journal for a color version of this figure.*]

4.3. *Estimating M/L_V^* and the Stellar Mass Density*

In this subsection, we describe the use of our mean cosmic color estimates to derive the mean cosmic M/L_V^* and the evolution in ρ_*.

The main strength of considering the luminosity density and integrated colors of the galaxy population, as opposed to those of individual galaxies, lies in the simple and robust ways in which these global values can be modeled. When attempting to derive the SFHs and stellar masses of individual high-redshift galaxies, the state-of-the-art models for the broadband colors only consider stellar populations with at most two separate components (SY98; P01; Shapley et al. 2001). Using their stellar population synthesis modeling, Shapley et al. (2001) propose a model in which LBGs likely have smooth SFHs. On the other hand, SY98 concluded that they may only be seeing the most recent episode of star formation and that LBGs may indeed have bursting SFHs. This same idea was supported by P01 and Ferguson, Dickinson, & Papovich (2002), using much deeper NIR data. When using similar simple SFHs to model the cosmic average of the galaxy population, a more self-consistent approach is possible. While individual galaxies may, and probably do, have complex SFHs, the mean SFH of all galaxies is much smoother than that of individual ones.

Encouraged by the general agreement between the measured colors and the simple models, we attempted to use this model to constrain the stellar mass-to-light ratio, M/L_V^*, in the rest-frame V band by taking advantage of the relation between color and $\log M/L^*$ found by Bell & de Jong (2001). For monotonic SFHs, the scatter of this relation remains small in the presence of modest variations in the reddening and metallicity, because these effects run roughly parallel to the mean relation. Using the $\tau = 6$ Gyr exponentially declining model, we plot in Figure 5 the relation between $(U-V)_{\rm rest}$ and M/L_V^* for the $E(B-V) = 0$, 0.15, and 0.35 models. It is seen that dust extinction moves objects roughly parallel to the model tracks, reddening their colors, but making them dimmer as well and hence increasing M/L_V^*. Nonetheless, extinction uncertainties are a major contributor to our errors in the determination of M/L_V^*. We chose to derive M/L_V^* from the $(U-V)_{\rm rest}$ color instead of from the $(B-V)_{\rm rest}$ color, because at blue colors, where our high-redshift points lie, $(B-V)_{\rm rest}$–derived M/L_V^* values are much more sensitive to the exact value of the extinction. This behavior likely stems from the fact that the $(U-V)_{\rm rest}$ color spans the Balmer/4000 Å break and hence is more age-sensitive than $(B-V)_{\rm rest}$. At the same time, while $(U-B)_{\rm rest}$ colors are even less sensitive to extinction than $(U-V)_{\rm rest}$, they are more susceptible to the effects of bursts.

We constructed our relation using a Salpeter (1955) IMF.[12] The adoption of a different IMF would simply change the zero point of this curve, leaving the relative M/L^* as a function of color, however, unchanged. As discussed in § 4.2, this model does not fit the redshift evolution

[12] We do not attempt to model an evolving IMF, although evidence for a top-heavy IMF at high redshifts has been presented by Ferguson et al. (2002).

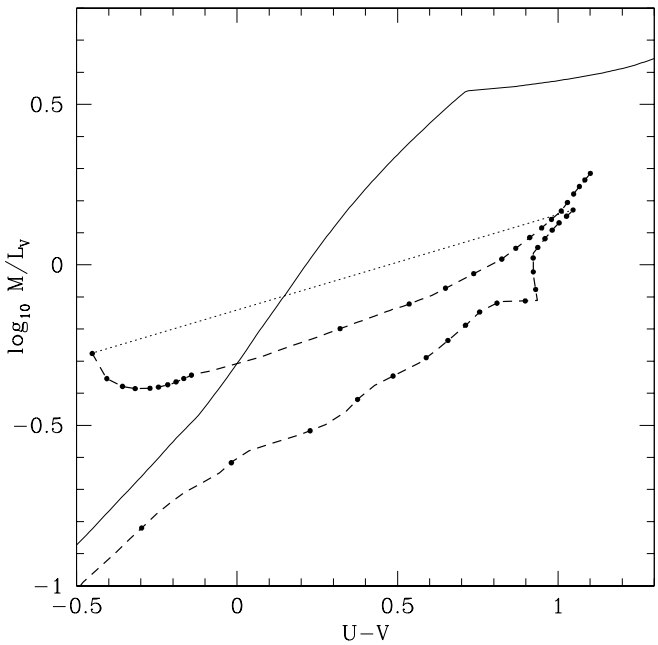

FIG. 6.—Effect of an early burst of star formation on the relation between $(U-V)$ and M/L_V^*. The relation between $(U-V)$ and M/L_V^* for a model track with an exponential timescale of 6 Gyr is shown by the solid line. We also show a track for an SFH that includes a 50 Myr burst at $t = 0$ followed by a gap of 2 Gyr and a constant SFR for 1 Gyr thereafter, where the fraction of mass formed in the burst is 0.5. The track continues for a total time of 4.5 Gyr. The circles are placed at 100 Myr intervals, and the dotted section of the line indicates the very rapid transition in color caused by the onset of the second period of star formation. Both tracks have the same extinction. [*See the electronic edition of the Journal for a color version of this figure.*]

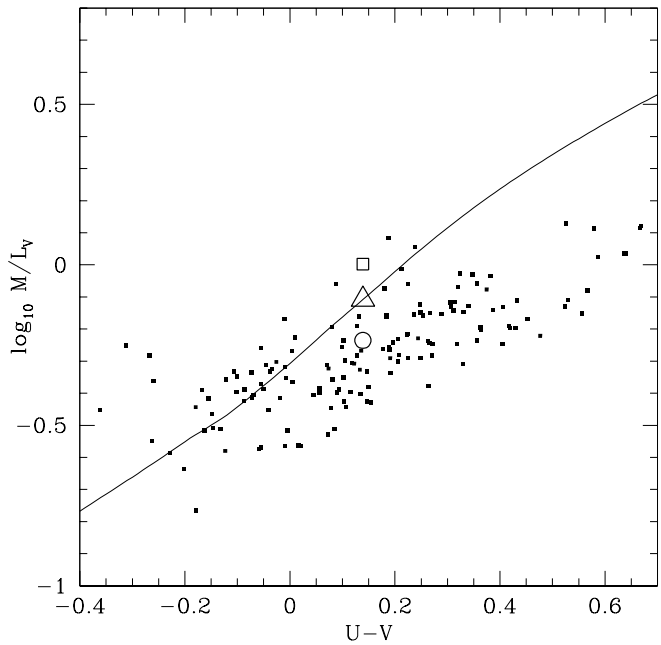

FIG. 7.—Comparison of different measures of the global M/L_V^* for a mock catalog of galaxies with bursting SFHs. The solid line represents the relation between $(U-V)$ and M/L_V^* for a model track with an exponential timescale of 6 Gyr. The filled squares show the true M/Ls of the model starbursting galaxies, as described in the text; the circle shows the true luminosity-weighted $M_{\rm tot}/L_{\rm tot}$ of the mock galaxies. The open square shows the luminosity-weighted M/L_V^* derived by applying the simple model to the individual galaxies—in this case, the mean $M_{\rm tot}/L_{\rm tot}$ is overestimated by 70%. The triangle shows the $M_{\rm tot}/L_{\rm tot}$ derived from the luminosity-weighted mean color [or $(U-V)_{\rm tot}$] of the model galaxies. It overestimates $M_{\rm tot}/L_{\rm tot}$ by only 35%. [*See the electronic edition of the Journal for a color version of this figure.*]

of the cosmic color very well. Nonetheless, the effect on our M/L_V^* estimates should not be very large, since most smooth SFHs occupy very similar positions in the M/L_V^* versus $U-V$ plane.

This relation breaks down in the presence of more complex SFHs. We demonstrate this in Figure 6, where we plot the $\tau = 6$ Gyr track and a second track whose SFH is comprised of a 50 Myr burst at $t = 0$, a gap of 2 Gyr, and a constant SFR for 1 Gyr thereafter, in which 50% of the mass is formed in the burst. It is obvious from this figure that using a smooth model will cause errors in the M/L_V^* estimate if the galaxy has an SFR that has an early peak in the SFH. At blue colors, such an early burst in the SFR will cause an underestimate of M/L_V^*, a result similar to that of P01 and D03. At red colors, however, M/L_V^* would be overestimated, with the exact systematic offset as a function of color depending strongly on the detailed SFH, i.e., the fraction of mass formed in the burst, the length of the gap, and the final age of the stellar population.

The models show that the method may over- or underestimate the true stellar mass-to-light ratio if the galaxies have complex SFHs. It is important to quantify the errors on the global M/L_V^* based on the mean $(U-V)_{\rm rest}$ color and how these errors compare to those when determining the global M/L_V^* value from individual M/L_V^* estimates. To make this comparison, we constructed a model whose SFH consists of a set of 10 Myr duration bursts separated by 90 Myr gaps. We drew galaxies at random from this model by randomly varying the phase and age of the burst sequence, where the maximum age was 4 Gyr. Next we estimated the total mass-to-light ratios of this sample by two different methods: (1) We determined the M/L_V^* for the galaxies, individually assuming the simple relation between color and mass-to-light ratio, and we took the luminosity-weighted mean of the individual estimates to obtain the total M/L_V^*. This point is indicated by a large square in Figure 7 and overestimates the total M/L_V^* by ~70%. (2) We first added the light of all the galaxies in both U and V and then used the simple relation between color and M/L_V^* to convert the integrated $(U-V)_{\rm rest}$ into a mass-to-light ratio. This method overestimates M/L_V^* by much less, ~35%. This comparison shows clearly that it is best to estimate the mass using the integrated light. This is not unexpected; the SFH of the universe as a whole is more regular than the SFH of individual galaxies. If enough galaxies are averaged, the mean SFH is naturally fairly smooth.

Using the relationship between color and M/L_V^*, we convert our $(U-V)_{\rm rest}$ and $j_V^{\rm rest}$ measurements to stellar mass density estimates ρ_*. The resulting ρ_* values are plotted versus cosmic time in Figure 8. We have included points for the SDSS survey created in a way analogous to those from this work, i.e., using the M/L_V^* derived from the rest-frame color and multiplying it by $j_V^{\rm SDSS}$ for all galaxies with $L_V^{\rm rest} > L_V^{\rm thresh}$. The ρ_* estimates are listed in Table 2. We have derived the statistical error bars on the ρ_* estimates by creating a Monte Carlo simulation in which we allowed $j_V^{\rm rest}$ and $(U-V)_{\rm rest}$ (and hence M/L_V^*) to vary within their error bars. We then took the resulting distribution of ρ_* values and determined the 68% confidence limits. As an estimate of

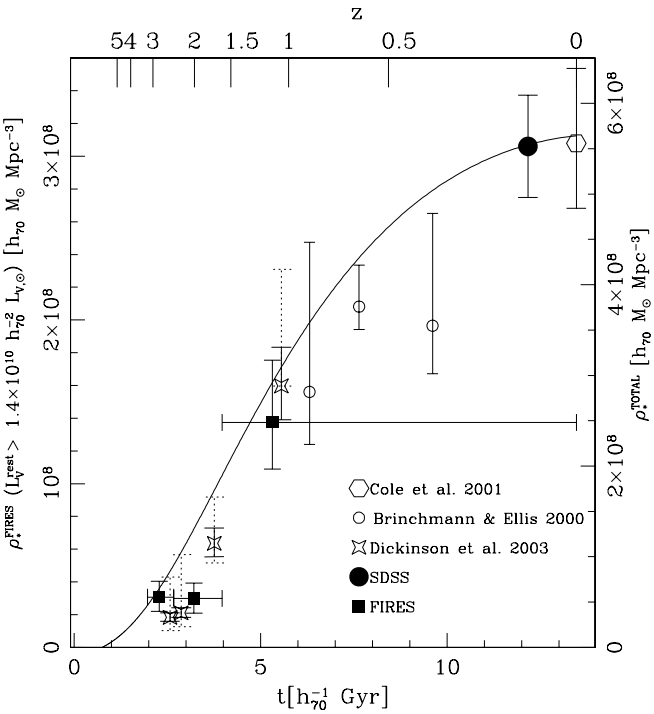

FIG. 8.—Buildup of stellar mass density as a function of redshift. The filled points are for galaxies with $L_V^{\rm rest} > 1.4 \times 10^{10}\ h_{70}^{-2}\ L_\odot$ and were derived by applying the $E(B-V) = 0.35$ relation in Fig. 5 to the $(U-V)_{\rm rest}$ colors and $j_\lambda^{\rm rest}$ measurements from the FIRES (*squares*) and SDSS data (*filled circle*). The *y*-axis scale on the left-hand side corresponds to the ρ_* values for these points. The open symbols show the total stellar mass density measurements from the one-component models in the HDF-N (D03; *stars*; calculated assuming solar metallicity), the CFRS (Brinchmann & Ellis 2000; *open circles*), and the 2dFGRS+2MASS (Cole et al. 2001; *hexagon*). The dotted error bars on the D03 points reflect the systematic mass uncertainties resulting from metallicity and SFH changes. The *y*-axis scale on the right-hand side corresponds to the ρ_* estimates for these points. The relative scaling of the two axes was adjusted so that our SDSS ρ_* estimate was at the same height as the total ρ_* estimate of Cole et al. The solid curve is an integral of the SFR(z) from Cole et al. (2001), which has been fitted to extinction-corrected data at $z \lesssim 4$. [*See the electronic edition of the Journal for a color version of this figure.*]

our systematic uncertainties corresponding to the method, we also determined M/L_V^* from the $(U-B)_{\rm rest}$ and $(B-V)_{\rm rest}$ data, using a relation identical to that for the $(U-V)_{\rm rest}$–to–M/L_V^* conversion. The $(U-B)_{\rm rest}$–derived M/L_V^* values were different from the $(U-V)_{\rm rest}$ values by a factor of 1.02, 0.80, 0.95, and 1.12 for the $z = 0.1$, 1.12, 2.01, and 2.8 redshift bins, respectively. Likewise, the $(B-V)_{\rm rest}$–determined M/L_V^* values changed by a factor of 0.99, 1.11, 1.15, and 0.80 with respect to the $(U-V)_{\rm rest}$ values. While the $(U-V)_{\rm rest}$ values are very similar to those derived from the other colors, the $(U-V)_{\rm rest}$ color is less susceptible to dust uncertainties than the $(B-V)_{\rm rest}$ data and less susceptible to the effects of bursts than the $(U-B)_{\rm rest}$ data.

The derived mass density rises monotonically by a factor of $\sim$10 all the way to $z \sim 0.1$, with our low-redshift point meshing nicely with the local SDSS point.

TABLE 2
M/L_V^* AND STELLAR MASS DENSITY ESTIMATES

Survey	z	$\log M/L_V^*$ $(M_\odot/L_\odot)$	$\log \rho_*$ $(h_{70}\ M_\odot\ {\rm Mpc}^{-3})$
SDSS	0.1 ± 0.1	0.54 ± 0.03	$8.49^{+0.04}_{-0.05}$
FIRES	$1.12^{+0.48}_{-1.12}$	$0.13^{+0.07}_{-0.06}$	$8.14^{+0.11}_{-0.10}$
	$2.01^{+0.40}_{-0.41}$	$-0.42^{+0.09}_{-0.10}$	$7.48^{+0.12}_{-0.16}$
	$2.80^{+0.40}_{-0.39}$	$-0.70^{+0.11}_{-0.12}$	$7.49^{+0.12}_{-0.14}$

NOTE.—Quantities are calculated for galaxies with $L_V^{\rm rest} > 1.4 \times 10^{10}\ h_{70}^{-2}\ L_\odot$.

5. DISCUSSION

5.1. *Comparison with Other Work*

Figure 8 shows a consistent picture of the buildup of stellar mass, both for the luminous galaxies and the total galaxy population. It is remarkable that the results from different authors appear to agree well, given that the methods to derive the densities were different and that the fields are very small.

We compared our results to the total mass estimates of other authors in Figure 8. In doing this we must remember that because of our $L_\lambda^{\rm thresh}$ cut, we are missing significant amounts of light, and hence mass. Assuming the SDSS luminosity function parameters, we lose 46% of the light at $z = 0$. At $z = 2.8$, however, we inferred a brightening of $L_{*,V}$ by a factor of 1.7, implying that we go farther down the luminosity function at high redshift, sampling a larger fraction of the total starlight. If we apply this brightening to the SDSS $L_{*,V}$, we miss 30% of the light below our luminosity threshold at $z = 2.8$. Hence, the fraction of the total starlight contained in our sample is rather stable as a function of redshift. To graphically compare our data to those of other authors, we have scaled the two different axes in Figure 8 so that our derivation of the SDSS ρ_* is at the same height as the total ρ_* estimate of Cole et al. (2001). At $z < 1$, we compared our mass estimates to those of Brinchmann & Ellis (2000). Following D03, we have corrected their published points to total masses by correcting them upward by 20% to account for their mass incompleteness. The fraction of the total stars formed at $z < 1$ agrees well between our data and those of SDSS and Brinchmann & Ellis. At $z > 0.5$, we compared our results to those of D03. D03 calculated the total mass density using the integrated luminosity density in the rest-frame B band, coupled with M/L measurements of individual galaxies. The fractions of the total stars formed in our sample (60%, 13%, and 9% at $z = 1.12$, 2.01, and 2.8, respectively) are almost twice as high as those of D03. The results, however, are consistent within the errors.

We explored whether field-to-field variations may play a role in the discrepancy between the two data sets. D03 studied the HDF-N, which has far fewer "red" galaxies than the HDF-S (e.g., Labbé et al. 2003; Franx et al. 2003). If we omit the $(J-K)$–selected galaxies found by Franx et al. (2003) in the HDF-S, the formal M/L_V^* decreases to 45% and 43% of the total values and the mass density decreases to 57% and 56% of the total values in the $z = 2.01$ and 2.8 bins, respectively, bringing our data into better agreement with those from D03. This reinforces the earlier suggestion by Franx et al. (2003) that the $(J-K)$–selected galaxies contribute significantly to the stellar mass budget.

The errors in both determinations are dominated by systematic uncertainties, although our method should be less sensitive to bursts than that of D03, as it uses the light integrated over the galaxy population.

We note that Fontana et al. (2003) have also measured the stellar mass density in the HDF-S, using a catalog derived from data in common with our own. They find a similar, although slightly smaller, evolution in the stellar mass density, consistent with our result within the uncertainties.

5.2. *Comparison with SFR(z)*

We can compare the derived stellar mass to the mass expected from determinations of the SFR as a function of redshift. We use the curve by Cole et al. (2001), who fitted the observed SFR as determined from various sources at $z \lesssim 4$. To obtain the curve in Figure 8, we integrated the SFR(z) curve, taking into account the time-dependent stellar mass loss derived from the 2000 version of the Bruzual A. & Charlot (1993) population synthesis models.

We calculated a reduced χ^2 of 4.3 when comparing all the data to the model. If, however, we omit the Brinchmann & Ellis (2000) data, the reduced χ^2 decreases to 1.8, although the results at $z > 2$ lie systematically below the curve. This suggests that some systematic errors may play a role or that the curve is not quite correct. The following sources of error can influence our mass density determinations:

Dusty, evolved populations.—It is assumed that the dust is mixed in a simple way with the stars, leading to a Calzetti extinction curve. If the dust is distributed differently, e.g., by having a very extincted underlying evolved population or by having a larger R-value, the current assumptions lead to a systematic underestimate of the mass. If an underlying, extincted, evolved population exists, it would naturally explain the fact that the ages of the LBGs are much younger than expected (e.g., P01; Ferguson et al. 2002). There may also be galaxies that contribute significantly to the mass density but are so heavily extincted that they are undetected, even with our very deep K_s-band data. If such objects are also actively forming stars, they may be detectable with deep submillimeter observations or with rest-frame NIR observations from *SIRTF*.

Cosmic variance.—The two fields that have been studied are very small. Although we use a consistent estimate of clustering from Daddi et al. (2003), red galaxies make up a large fraction of the mass density in our highest redshift bins. Since red galaxies have a very high measured clustering from $z \sim 1$ (e.g., Daddi et al. 2000; McCarthy et al. 2001) up to possibly $z \sim 3$ (Daddi et al. 2003), large uncertainties remain.

Evolving IMF.—The light that we see is mostly coming from the most massive stars present, whereas the stellar mass is dominated by low-mass stars. Changes in the IMF would immediately lead to different mass estimates, but if the IMF everywhere is identical (as we assume), then the relative masses should be robust. If the IMF evolves with redshift, however, systematic errors in the mass estimate will occur.

A steep galaxy mass function at high redshift.—If much of the UV light that is used to measure the SFR at high redshifts comes from small galaxies that would fall below our rest-frame luminosity threshold, then we may be missing significant amounts of stellar mass. Even the mass estimates of D03, which were obtained by integrating the luminosity function, are very sensitive to the faint-end extrapolation in their highest redshift bin.

5.3. *The Buildup of the Stellar Mass*

The primary goal of measuring the stellar mass density is to determine how rapidly the universe assembled its stars. At $z \sim 2$–3, our results indicate that the universe only contained $\sim$10% of the current stellar mass, regardless of whether we refer only to galaxies at $L_V^{\rm rest} > 1.4 \times 10^{10}\ h_{70}^{-2}\ L_\odot$ or use the total mass estimates of other authors. The galaxy population in the HDF-S was rich and diverse at $z > 2$, but even so it was far from finished in its buildup of stellar mass. By $z \sim 1$, however, the total mass density had increased to roughly half its local value, indicating that the epoch of $1 < z < 2$ was an important period in the stellar mass buildup of the universe.

A successful model of galaxy formation must not only explain our global results but also reconcile them with the observed properties of individual galaxies at all redshifts. For example, a population of galaxies at $z \sim 1$–1.5 has been discovered (the so-called extremely red objects, or EROs), roughly half of which can be fitted with formation redshifts higher than 2.4 (Cimatti et al. 2002) and nearly passive stellar evolution thereafter. Our results, which show that the universe contained only $\sim$10% as many stars at $z \sim 2$–3 as today, would seem to indicate that any population of galaxies that formed most of its mass at $z \gtrsim 2$ can *at most* contribute $\sim$10% of the present-day stellar mass density. At $z \sim 1$–1.5, where the EROs reside, the universe had assembled roughly half of its current stars. Therefore, this would imply that the old EROs contribute about $\sim$20% of the mass budget at their epoch. Likewise, it should be true that a large fraction of the stellar mass at low redshift should reside in objects with mass-weighted stellar ages corresponding to a formation redshift of $1 < z < 2$. In support of this, Hogg et al. (2002) recently have shown that $\sim$40% of the local luminosity density at 0.7 μm, and perhaps $\sim$50% of the stellar mass, comes from centrally concentrated, high surface brightness galaxies that have red colors. In agreement with the Hogg et al. (2002) results, Bell et al. (2003a) and Kauffmann et al. (2003) also found that $\sim$50%–75% of the local stellar mass density resides in early-type galaxies. Hogg et al. (2002) suggest that their red galaxies would have been formed at $z \gtrsim 1$, fully consistent with our results for the rapid mass growth of the universe during this period.

6. SUMMARY AND CONCLUSIONS

In this paper we presented the globally averaged rest-frame optical properties of a K_s band–selected sample of galaxies with $z < 3.2$ in the HDF-S. Using our very deep 0.3–2.2 μm, seven-band photometry taken as part of the FIRE Survey, we estimated accurate photometric redshifts and rest-frame luminosities for all galaxies with $K_{s,\rm AB}^{\rm tot} < 25$ and used these luminosity estimates to measure the rest-frame optical luminosity density, $j_\lambda^{\rm rest}$, the globally averaged rest-frame optical color, and the stellar mass density for all galaxies at $z < 3.2$ with $L_V^{\rm rest} > 1.4 \times 10^{10}\ h_{70}^{-2}\ L_\odot$. By selecting galaxies in the rest-frame V band, we selected them in a way much less biased by star formation and dust than the traditional selection in the rest-frame UV and much closer to a selection by stellar mass.

We have shown that $j_\lambda^{\rm rest}$ in all three bands rises out to $z \sim 3$ by factors of 4.9 ± 1.0, 2.9 ± 0.6, and 1.9 ± 0.4 in the U, B, and V bands, respectively. Modeling this increase in $j_\lambda^{\rm rest}$ as an increase in L_* of the local luminosity function, we

derive that L_* must have brightened by a factor of 1.7 in the rest-frame V band.

Using our $j_\lambda^{\rm rest}$ estimates, we calculate the $(U-B)_{\rm rest}$ and $(B-V)_{\rm rest}$ colors of all the visible stars in galaxies with $L_V^{\rm rest} > 1.4 \times 10^{10}\ h_{70}^{-2}\ L_\odot$. Using the COMBO-17 data, we have shown that the mean color is much less sensitive to density fluctuations and field-to-field variations than either $j_\lambda^{\rm rest}$ or ρ_*. Because of their stability, integrated color measurements are ideal for constraining galaxy evolution models. The luminosity-weighted mean colors lie close to the locus of morphologically normal local galaxy colors defined by Larson & Tinsley (1978). The mean colors monotonically bluen with increasing redshift by 0.55 and 0.46 mag in $(U-B)_{\rm rest}$ and $(B-V)_{\rm rest}$, respectively, out to $z \sim 3$. We interpret this color change primarily as a change in the mean stellar age. The joint colors can be roughly matched by simple SFH models if modest amounts of reddening [$E(B-V) < 0.35$] are applied. In detail, the redshift dependence of $(U-B)_{\rm rest}$ and $(B-V)_{\rm rest}$ cannot be matched exactly by the simple models, assuming a constant reddening and constant metallicity. However, we show that the models can still be used, even in the face of these small disagreements, to robustly predict the stellar mass-to-light ratios M/L_V^* of the integrated cosmic stellar population implied by our mean rest-frame colors. Variations in the metallicity do not strongly affect this relation, and it holds for a variety of smooth SFHs. Even the IMF only affects the normalization of this relation, not its slope, assuming that the IMF everywhere is the same. The reddening, which moves objects roughly along this relation, is, however, a large source of uncertainty. Using these M/L_V^* estimates coupled with our $j_\lambda^{\rm rest}$ measurements, we derive the stellar mass density, ρ_*. These globally averaged estimates of the mass density are more reliable than those obtained from the mean of individual galaxies determined using smooth SFHs, primarily because the cosmic mean SFH is plausibly much better approximated as being smooth, whereas the SFHs of individual galaxies are almost definitely not.

The stellar mass density, ρ_*, increases monotonically with increasing cosmic time to come into good agreement with the other measured values at $z \lesssim 1$, with a factor of $\sim$10 increase from $z \sim 3$ to the present day. Within the random uncertainties, our results agree well with those of D03 in the HDF-N, although our ρ_* estimates are systematically higher than in the HDF-N. Taken together, the HDF-N and HDF-S paint a picture in which only $\sim$5%–15% of the present-day stellar mass was formed by $z \sim 2$. By $z \sim 1$, however, the stellar mass density had increased to $\sim$50% of its present value, implying that a large fraction of the stellar mass in the universe today was assembled at $1 < z < 2$. Our ρ_* estimates slightly underpredict the stellar mass density derived from the integral of the SFR(z) curve at $z > 2$. A resolution of the small apparent discrepancy between different fields and that between the predictions from optical observations will in part require deeper NIR data, to probe farther down the mass function, and wider fields with multiple pointings, to control the effects of cosmic variance. In addition, large amounts of follow-up optical/NIR spectroscopy are required to help control systematic effects in the $z_{\rm phot}$ estimates. The 25 arcmin^2 MS 1054-03 data taken as part of FIRES and the ACS/ISAAC GOODS observations of the *Chandra* Deep Field–South (CDF-S) region will be very helpful for such studies. Observations with *SIRTF* will also improve the situation by accessing the rest-frame NIR, where obscuration by dust becomes much less important. Finally, systematics in the M/L^* estimates may exist because of a lack of constraint on the faint-end slope of the stellar IMF.

We still have to reconcile global measurements of the galaxy population with what we know about the ages and SFHs of individual galaxies. Our globally determined quantities are quite stable and may serve as robust constraints on theoretical models, which must correctly model the global buildup of stellar mass, in addition to matching the detailed properties of the galaxy population.

G. R. would like to thank Jarle Brinchmann and Frank van den Bosch for useful discussions in the process of writing this paper, Christian Wolf for providing additional COMBO-17 data products, and Eric Bell and Marcin Sawicki for giving comments on an earlier version of the paper. G. R. would also like to acknowledge the generous travel support of the Lorentz center and the Leids Kerkhoven-Bosscha Fonds and the financial support of Sonderforschungsbereich 375. Funding for the creation and distribution of the SDSS Archive has been provided by the Alfred P. Sloan Foundation, the Participating Institutions, the National Aeronautics and Space Administration, the National Science Foundation, the US Department of Energy, the Japanese Monbukagakusho, and the Max Planck Society. The SDSS Web site is http://www.sdss.org. The SDSS is managed by the Astrophysical Research Consortium (ARC) for the Participating Institutions. The Participating Institutions are the University of Chicago, Fermilab, the Institute for Advanced Study, the Japan Participation Group, The Johns Hopkins University, Los Alamos National Laboratory, the Max Planck Institute for Astronomy (MPIA), the Max Planck Institute for Astrophysics (MPA), New Mexico State University, University of Pittsburgh, Princeton University, the United States Naval Observatory, and the University of Washington.

APPENDIX A

DERIVATION OF $z_{\rm phot}$ UNCERTAINTY

Given a set of formal flux errors, one way to broaden the redshift confidence interval without degrading the accuracy (as noted in R01) is to lower the absolute χ^2 of every $\chi^2(z)$ curve without changing its shape (or the location of the minimum). By scaling up all the flux errors by a constant factor, we can retain the relative weights of the points in the χ^2 without changing the best-fit redshift and SED, but we do enlarge the redshift interval over which the templates can satisfactorily fit the flux points. Since we believe that the disagreement between $z_{\rm spec}$ and $z_{\rm phot}$ is due to our finite and incomplete template set, this factor should reflect the degree of template mismatch in our sample, i.e., the degree by which our models fail to fit the flux points. To estimate

this factor, we first compute the fractional difference between the model and the data $\Delta_{i,j}$ for the jth galaxy in the ith filter,

$$\Delta_{i,j} = \frac{(f_{i,j}^{\rm mod} - f_{i,j}^{\rm dat})}{f_{i,j}^{\rm dat}} , \tag{A1}$$

where $f^{\rm mod}$ are the predicted fluxes of the best-fit template combination and $f^{\rm dat}$ are our actual data. For each galaxy we calculated

$$\Delta_j = \sqrt{\frac{1}{N_{\rm filt} - 1} \sum_{i=2}^{N_{\rm filt}} \Delta_{i,j}^2} , \tag{A2}$$

where we have ignored the contributions of the U band. While the U band is important in finding breaks in the SEDs, the exact shapes of the templates are poorly constrained blueward of the rest-frame U band, and the U-band data often deviate significantly from the best-fit model fluxes.

To determine the mean deviation of all of the flux points from the model $\Delta_{\rm dev}$, we then averaged over all galaxies in our complete FIRES sample with $K_{s,{\rm AB}}^{\rm tot} < 22$ (for which the systematic $z_{\rm phot}$ errors should dominate over those resulting from photometric errors), to obtain

$$\Delta_{\rm dev} = \frac{1}{N_{\rm gal}} \sum_{j=1}^{N_{\rm gal}} |\Delta_j| . \tag{A3}$$

We find $\Delta_{\rm dev} = 0.08$, which includes both random and systematic deviations from the model. We modified the Monte Carlo simulation of R01 by calculating, for each object j,

$$\langle {\rm S/N} \rangle_j = \sqrt{\frac{\sum_{i=2}^{N_{\rm filt}} (f_i/\delta f_i)^2}{N_{\rm filt} - 1}} , \tag{A4}$$

again excluding the U band. We then scaled the flux errors for each object, using the following criteria:

$$\delta f_i' = \begin{cases} \delta f_i & \langle {\rm S/N} \rangle_j \leq \dfrac{1}{\Delta_{\rm dev}} \\ \delta f_i \Delta_{\rm dev} \langle {\rm S/N} \rangle_j & \langle {\rm S/N} \rangle_j > \dfrac{1}{\Delta_{\rm dev}} \end{cases} \tag{A5}$$

The photometric redshift error probability distribution is computed using the $\delta f_i'$ values. Note that this procedure will not modify the $z_{\rm phot}$ errors of the objects with low signal-to-noise ratio (S/N), where the $z_{\rm phot}$ errors are dominated by the formal photometric errors. The resulting probability distribution is highly non-Gaussian, and using it we calculate the upper and lower 68% confidence limits on the redshift $z_{\rm phot}^{\rm hi}$ and $z_{\rm phot}^{\rm low}$, respectively. As a single number that encodes the total range of acceptable $z_{\rm phot}$ values, we define $\delta z_{\rm phot} \equiv 0.5(z_{\rm phot}^{\rm hi} - z_{\rm phot}^{\rm low})$.

Figure 6 of L03 shows the comparison of $z_{\rm phot}$ to $z_{\rm spec}$. For these bright galaxies, it is remarkable that our new photometric redshift error bars come so close to predicting the difference between $z_{\rm phot}$ and the true value. Some galaxies have large $\delta z_{\rm phot}$ values even when the local χ^2 minimum is well defined, because there is another χ^2 minimum of comparable depth that is contained in the 68% redshift confidence limits. There are galaxies with $\delta z_{\rm phot} < 0.05$. Some of these are bright, low-redshift galaxies with large rest-frame optical breaks, which presumably place a strong constraint on the allowed redshift. Many of these galaxies, however, are faint, and the $\delta z_{\rm phot}$ is unrealistically low. Even though these faint galaxies have $\langle {\rm S/N} \rangle_j \leq 1/\Delta_{\rm dev}$, they still can have high S/Ns in the B_{450} or V_{606} bandpasses and hence have steep χ^2 curves and small inferred redshift uncertainties. In addition, many of these galaxies have $z_{\rm phot} > 2$ and very blue continua longward of Lyα. The imposed sharp discontinuity in the template SEDs at the onset of H I absorption causes a very narrow minimum in the $\chi^2(z)$ curve, and hence a small $\delta z_{\rm phot}$, but likely differs from the true shape of the discontinuity, because we use the mean opacity values of Madau (1995), neglecting its variance among different lines of sight.

It is difficult to develop a scheme for measuring realistic photometric redshift uncertainties over all regimes. The $\delta z_{\rm phot}$ estimate derives the $z_{\rm phot}$ uncertainties individually for each object, but it can underpredict the uncertainties in some cases. Compared to the technique of R01, however, a method based completely on the Monte Carlo technique is preferable, because it has a straightforwardly computed redshift probability function. This trait is desirable for estimating the errors in the rest-frame luminosities and colors, and for this reason we use $\delta z_{\rm phot}$ as our uncertainty estimate in this paper.

APPENDIX B

REST-FRAME PHOTOMETRIC SYSTEM

To define the rest-frame U, B, and V fluxes, we use the filter transmission curves and zero points tabulated in Bessell (1990), specifically, his UX, B, and V filters. The Bessell zero points are given as magnitude offsets with respect to a source that has

constant f_ν and AB = 0. The AB magnitude is defined as

$$\mathrm{AB}_\nu = -2.5\log_{10}\langle f_\nu\rangle - 48.58 \ , \tag{B1}$$

where $\langle f_\nu\rangle$ is the flux $f_\nu(\nu)$ observed through a filter $T(\nu)$ in units of ergs s^{-1} cm^{-2} Hz^{-1}. Given the zero-point offset ZP_ν for a given filter, the Vega magnitude m_ν is then

$$m_\nu = \mathrm{AB}_\nu - \mathrm{ZP}_\nu = -2.5\log_{10}\langle f_\nu\rangle - 48.58 - \mathrm{ZP}_\nu \ . \tag{B2}$$

All of our observed fluxes and rest-frame template fluxes are expressed in f_λ. To obtain rest-frame magnitudes in the Bessell (1990) system, we must calculate the conversion from f_λ to f_ν for the redshifted rest-frame filter set. The flux density of an SED with $f_\lambda(\lambda)$ integrated through a given filter with transmission curve $T(\lambda)$ is

$$\langle f_\lambda\rangle = \frac{\int f_\lambda(\lambda')T'(\lambda')\,d\lambda'}{\int T'(\lambda')\,d\lambda'} \ , \tag{B3}$$

or

$$\langle f_\nu\rangle = \frac{\int f_\nu(\nu')T'(\nu')\,d\nu'}{\int T'(\nu')\,d\nu'} \ . \tag{B4}$$

Since

$$\int f_\lambda(\lambda')T'(\lambda')\,d\lambda' = \int f_\nu(\nu')T'(\nu')\,d\nu' \ , \tag{B5}$$

we can convert to $\langle f_\nu\rangle$ through

$$\langle f_\nu\rangle = \langle f_\lambda\rangle\,\frac{\int T'(\lambda')\,d\lambda'}{\int T'(\nu')\,d\nu'} \tag{B6}$$

and use $\langle f_\nu\rangle$ to calculate the apparent rest-frame Vega magnitude through the redshifted filter via equation (B2).

APPENDIX C

ESTIMATING REST-FRAME LUMINOSITIES

We derive, for any given redshift, the relation between the apparent AB magnitude m_{λ_z} of a galaxy through a redshifted rest-frame filter, its observed fluxes $\langle f_{\lambda_i,\mathrm{obs}}\rangle$ in the different filters i, and the colors of the spectral templates. At redshift z, the rest-frame filter with effective wavelength λ_{rest} has been shifted to an observed wavelength

$$\lambda_z = \lambda_{\mathrm{rest}}(1+z) \ , \tag{C1}$$

and we define the adjacent observed bandpasses with effective wavelengths λ_l and λ_h, which satisfy

$$\lambda_l < \lambda_z \leq \lambda_h \ . \tag{C2}$$

We now define

$$C_{\mathrm{obs}} \equiv m_{\mathrm{obs},\lambda_l} - m_{\mathrm{obs},\lambda_h} \ , \tag{C3}$$

where $m_{\mathrm{obs},\lambda_l}$ and $m_{\mathrm{obs},\lambda_h}$ are the AB magnitudes that correspond to the fluxes $\langle f_{\lambda_l,\mathrm{obs}}\rangle$ and $\langle f_{\lambda_h,\mathrm{obs}}\rangle$, respectively. We then shift each template in wavelength to the redshift z and compute

$$C_{\mathrm{templ}} \equiv m_{\mathrm{templ},\lambda_l} - m_{\mathrm{templ},\lambda_h} \ , \tag{C4}$$

where $m_{\mathrm{templ},\lambda_l}$ and $m_{\mathrm{templ},\lambda_h}$ are the AB magnitudes through the λ_l and λ_h observed bandpasses (including the atmospheric and instrument throughputs), respectively. We sort the templates by their C_{templ} values, $C_{\mathrm{templ},a}$, $C_{\mathrm{templ},b}$, etc., and find the two templates such that

$$C_{\mathrm{templ},a} \leq C_{\mathrm{obs}} < C_{\mathrm{templ},b} \ . \tag{C5}$$

We then define, for the ath template,

$$C_{\lambda_l,z,a} \equiv m_{\mathrm{templ},\lambda_l} - m_{\mathrm{templ},\lambda_z} \ , \tag{C6}$$

where $m_{\mathrm{templ},\lambda_z}$ is the apparent AB magnitude of the redshifted ath template through the redshifted λ_{rest} filter. We point out that because our computations always involve colors, they are not dependent on the actual template normalization (which cancels out in the difference). Taking our observed color C_{obs} and the templates with adjacent "observed" colors $C_{\mathrm{templ},a}$ and

$C_{\mathrm{templ},b}$, we can interpolate between $C_{\lambda_l,z,a}$ and $C_{\lambda_l,z,b}$,

$$m_{\mathrm{obs},\lambda_l} - m_{\lambda_z} = C_{\lambda_l,z,a} + \left(C_{\mathrm{obs}} - C_{\mathrm{templ},a}\right)\left(\frac{C_{\lambda_l,z,b} - C_{\lambda_l,z,a}}{C_{\mathrm{templ},b} - C_{\mathrm{templ},a}}\right), \tag{C7}$$

and solve for m_{λ_z}.

When C_{obs} lies outside the range of C_{templ}, we simply take the two nearest templates in observed C_{templ} space and extrapolate equation (C7) to compute m_{λ_z}.

Equation (C7) has the feature that $m_{\lambda_z} \approx m_{\mathrm{obs},\lambda_l}$ when $\lambda_z = \lambda_l$ (and hence when $C_{\lambda_l,z,a}$ and $C_{\lambda_l,z,b} \approx 0$). While this method still assumes that the templates are reasonably good approximations to the true shape of the SEDs, it has the advantage that it does not rely on exact agreement. Galaxies whose observed colors fall outside the range of the templates can also be easily flagged. A final advantage of this method is that the uncertainty in m_{λ_z} can be readily calculated from the errors in the observed fluxes.

From m_{λ_z}, we compute the rest-frame luminosity by applying the K-correction and converting to luminosity units:

$$\frac{L_\lambda^{\mathrm{rest}}}{L_\odot} = 10^{-0.4\left(m_{\lambda_z} - M_{\odot,\lambda_{\mathrm{rest}}} - \mathrm{ZP}_{\lambda_{\mathrm{rest}}}\right)}\left(\frac{D_L}{10\ \mathrm{pc}}\right)^2 (1+z)^{-1}\ h^{-2}, \tag{C8}$$

where $M_{\odot,\lambda_{\mathrm{rest}}}$ is the absolute magnitude of the Sun in the λ_{rest} filter ($M_{\odot,U} = +5.66$, $M_{\odot,B} = +5.47$, and $M_{\odot,V} = +4.82$ in Vega magnitudes; Cox 2000), $\mathrm{ZP}_{\lambda_{\mathrm{rest}}}$ is the zero point in that filter (as in eq. [B2] but expressed at λ and not at ν), and D_L is the distance modulus in parsecs. Following R01, we correct this luminosity by the ratio of the K_s^{tot} flux to the modified isophotal aperture flux (see L03). This adjustment factor, which accounts for both the larger size of the total aperture and the aperture correction, changes with apparent magnitude, ranges from 1.23 at $20 < K_{s,\mathrm{AB}}^{\mathrm{tot}} \leq 24$ to 1.69 at $24 < K_{s,\mathrm{AB}}^{\mathrm{tot}} \leq 25$, and has rms dispersions of 0.17 and 0.49 in the two magnitude bins, respectively.

The uncertainty in the derived $L_\lambda^{\mathrm{rest}}$ has contributions from both the observational flux errors and the redshift uncertainty, which causes λ_z to move with respect to the observed filters. The first effect is estimated by propagating the observed flux errors through equation (C7). As an example, object 531, at $z_{\mathrm{phot}} = 2.20$, has $K_{s,\mathrm{AB}}^{\mathrm{tot}} = 24.91$ and S/N in the K_s band of 8.99 and 5.43 in our modified isophotal and total apertures, respectively. The resultant error in L_V^{rest} purely from flux errors is then 26%. At $K_{s,\mathrm{AB}}^{\mathrm{tot}} \approx 24$, the typical S/N in the K_s band increases to $\approx$13 and $\approx$6.3 in our modified isophotal and total apertures, respectively, and the error $L_\lambda^{\mathrm{rest}}$ decreases accordingly.

To account for the redshift-dependent error in the calculated luminosity, we use the Monte Carlo simulation described first in R01 and updated in Appendix A. For each Monte Carlo iteration, we calculate the rest-frame luminosities and determine the 68% confidence limits of the resulting distribution. The 68% confidence limits in $L_\lambda^{\mathrm{rest}}$ can be highly asymmetric, just as for z_{phot}. For objects with $K_{s,\mathrm{AB}}^{\mathrm{tot}} \lesssim 25$, we find that the contributions to the total $L_\lambda^{\mathrm{rest}}$ error budget are dominated by the redshift errors, rather than by the flux errors.

REFERENCES

Baldry, I. K., et al. 2002, ApJ, 569, 582
Bell, E. F., & de Jong, R. S. 2001, ApJ, 550, 212
Bell, E. F., McIntosh, D. H., Katz, N., & Weinberg, M. D. 2003a, ApJ, 585, L117
Bell, E. F., Wolf, C., Meisenheimer, K., Rix, H.-W., Borch, A., Dye, S., Kleinheinrich, K., & McIntosh, D. H. 2003b, ApJ, submitted (astro-ph/0303394)
Benítez, N., Broadhurst, T., Bouwens, R., Silk, J., & Rosati, P. 1999, ApJ, 515, L65
Bertin, E., & Arnouts, S. 1996, A&AS, 117, 393
Bessell, M. S. 1990, PASP, 102, 1181
Bessell, M. S., & Brett, J. M. 1988, PASP, 100, 1134
Blanton, M. R., et al. 2001, AJ, 121, 2358
———. 2003a, AJ, 125, 2348
———. 2003b, ApJ, 592, 819 (B03)
———. 2003c, ApJ, 594, 186
Bolzonella, M., Pelló, R., & Maccagni, D. 2002, A&A, 395, 443
Brinchmann, J., & Ellis, R. S. 2000, ApJ, 536, L77
Bruzual A., G., & Charlot, S. 1993, ApJ, 405, 538
Calzetti, D., Armus, L., Bohlin, R. C., Kinney, A. L., Koornneef, J., & Storchi-Bergmann, T. 2000, ApJ, 533, 682
Casertano, S., et al. 2000, AJ, 120, 2747
Charlot, S., & Longhetti, M. 2001, MNRAS, 323, 887
Chen, H.-W., et al. 2003, ApJ, 586, 745
Cimatti, A., et al. 2002, A&A, 381, L68
Cole, S., et al. 2001, MNRAS, 326, 255
Colless, M., et al. 2001, MNRAS, 328, 1039
Cowie, L. L., Songaila, A., & Barger, A. J. 1999, AJ, 118, 603
Cox, A. N., ed. 2000, Allen's Astrophysical Quantities, (4th ed.; New York: Springer)
Cristiani, S., et al. 2000, A&A, 359, 489
Daddi, E., Cimatti, A., Pozzetti, L., Hoekstra, H., Röttgering, H. J. A., Renzini, A., Zamorani, G., & Mannucci, F. 2000, A&A, 361, 535
Daddi, E., et al. 2003, ApJ, 588, 50
Dickinson, M., Papovich, C., Ferguson, H. C., & Budavári, T. 2003, ApJ, 587, 25 (D03)
Erb, D. K., Shapley, A. E., Steidel, C. C., Pettini, M., Adelberger, K. L., Hunt, M. P., Moorwood, A. F. M., & Cuby, J.-G. 2003, ApJ, 591, 101
Ferguson, H. C., Dickinson, M., & Papovich, C. 2002, ApJ, 569, L65
Folkes, S., et al. 1999, MNRAS, 308, 459
Fontana, A., D'Odorico, S., Poli, F., Giallongo, E., Arnouts, S., Cristiani, S., Moorwood, A., & Saracco, P. 2000, AJ, 120, 2206
Fontana, A., et al. 2003, ApJ, 594, L9
Franx, M., et al. 2003, ApJ, 587, L79
Fried, J. W., et al. 2001, A&A, 367, 788
Giavalisco, M., & Dickinson, M. 2001, ApJ, 550, 177
Glazebrook, K., et al. 2003, ApJ, 587, 55
Hauschildt, P. H., Allard, F., & Baron, E. 1999, ApJ, 512, 377
Hogg, D. W., et al. 2002, AJ, 124, 646
Jansen, R. A., Fabricant, D., Franx, M., & Caldwell, N. 2000a, ApJS, 126, 331
Jansen, R. A., Franx, M., Fabricant, D., & Caldwell, N. 2000b, ApJS, 126, 271
Kashikawa, N., et al. 2003, AJ, 125, 53
Kauffmann, G., et al. 2003, MNRAS, 341, 33
Labbé, I., et al. 2003, AJ, 125, 1107 (L03)
Lanzetta, K. M., Yahata, N., Pascarelle, S., Chen, H.-W., & Fernández-Soto, A. 2002, ApJ, 570, 492
Larson, R. B., & Tinsley, B. M. 1978, ApJ, 219, 46
Lilly, S. J., Le Fèvre, O., Hammer, F., & Crampton, D. 1996, ApJ, 460, L1
Madau, P. 1995, ApJ, 441, 18
Madau, P., Ferguson, H. C., Dickinson, M. E., Giavalisco, M., Steidel, C. C., & Fruchter, A. 1996, MNRAS, 283, 1388
Madau, P., Pozzetti, L., & Dickinson, M. 1998, ApJ, 498, 106
McCarthy, P. J., et al. 2001, ApJ, 560, L131
Moorwood, A. F. 1997, Proc. SPIE, 2871, 1146
Norberg, P., et al. 2002, MNRAS, 336, 907
Papovich, C., Dickinson, M., & Ferguson, H. C. 2001, ApJ, 559, 620 (P01)
Pei, Y. C., Fall, S. M., & Hauser, M. G. 1999, ApJ, 522, 604
Pettini, M., Rix, S. A., Steidel, C. C., Adelberger, K. L., Hunt, M. P., & Shapley, A. E. 2002, ApJ, 569, 742

Pettini, M., Shapley, A. E., Steidel, C. C., Cuby, J.-G., Dickinson, M., Moorwood, A. F. M., Adelberger, K. L., & Giavalisco, M. 2001, ApJ, 554, 981
Pettini, M., Steidel, C. C., Adelberger, K. L., Dickinson, M., & Giavalisco, M. 2000, ApJ, 528, 96
Poli, F., Menci, N., Giallongo, E., Fontana, A., Cristiani, S., & D'Odorico, S. 2001, ApJ, 551, L45
Poli, F., et al. 2003, ApJ, 593, L1
Rigopoulou, D., et al. 2000, ApJ, 537, L85
Rudnick, G., et al. 2001, AJ, 122, 2205 (R01)
Salpeter, E. E. 1955, ApJ, 121, 161
Sawicki, M. J., Lin, H., & Yee, H. K. C. 1997, AJ, 113, 1
Sawicki, M. J., & Yee, H. K. C. 1998, AJ, 115, 1329 (SY98)
Shapley, A. E., Steidel, C. C., Adelberger, K. L., Dickinson, M., Giavalisco, M., & Pettini, M. 2001, ApJ, 562, 95
Skrutskie, M. F., et al. 1997, in The Impact of Large Scale Near-IR Sky Surveys, ed. F. Garzón, N. Epchtein, A. Omont, B. Burton, & P. Persi (Dordrecht: Kluwer), 25
Steidel, C. C., Adelberger, K. L., Giavalisco, M., Dickinson, M., & Pettini, M. 1999, ApJ, 519, 1
Steidel, C. C., Giavalisco, M., Pettini, M., Dickinson, M., & Adelberger, K. L. 1996, ApJ, 462, L17
Stoughton, C., et al. 2002, AJ, 123, 485
Strauss, M. A., et al. 2002, AJ, 124, 1810
Thompson, R. I. 2003, ApJ, 596, 748
Thompson, R. I., Weymann, R. J., & Storrie-Lombardi, L. J. 2001, ApJ, 546, 694
van Dokkum, P. G., Franx, M., Kelson, D. D., & Illingworth, G. D. 2001, ApJ, 553, L39
van Dokkum, P. G., et al. 2003, ApJ, 587, L83
Vanzella, E., et al. 2002, A&A, 396, 847
Wilson, G., Cowie, L. L., Barger, A. J., & Burke, D. J. 2002, AJ, 124, 1258
Wolf, C., Meisenheimer, K., Rix, H.-W., Borch, A., Dye, S., & Kleinheinrich, M. 2003, A&A, 401, 73
York, D. G., et al. 2000, AJ, 120, 1579
Zepf, S. E. 1997, Nature, 390, 377